AD-A053 251 LOUISIANA STATE UNIV BATON ROUGE COASTAL STUDIES INST F/G 8/3
SHALLOW-WATER WAVES AND FLUID-MUD DYNAMICS, COAST OF SURINAM, S--ETC(U)
APR 78 J T WELLS N00014-75-C-0192
UNCLASSIFIED TR-257 NL

1 OF 1
AD
A053251

END
DATE
FILMED
6-78
DDC

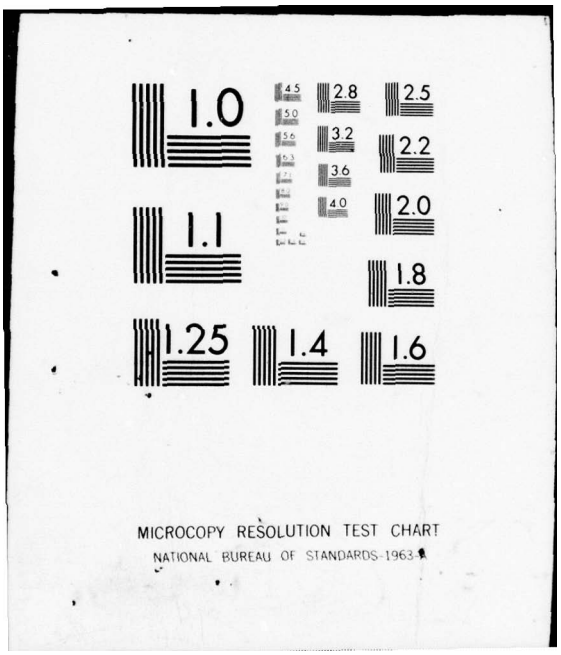
1.0
1.1
1.25
1.4
1.6
1.8
2.0
2.2
2.5
2.8
3.2
3.6
4.0
4.5
5.0
5.6
6.3
MICROCOPY RESOLUTION TEST CHART
NATIONAL BUREAU OF STANDARDS-1963-A

Center for Wetland Resources
Louisiana State University
Baton Rouge, Louisiana 70803

Technical Report No. 257

SHALLOW-WATER WAVES AND FLUID-MUD DYNAMICS, COAST OF SURINAM, SOUTH AMERICA

By John T. Wells

This research is supported by the Office of Naval Research through Cont
N00014-75-C-0192, under Project NR 388 002.

April 1978

Coastal Studies Institute
Center for Wetland Resources
Louisiana State University
Baton Rouge, Louisiana 70803

Technical Report No. 257

SHALLOW-WATER WAVES AND FLUID-MUD DYNAMICS, COAST OF SURINAM, SOUTH AMERICA

By John T. Wells

April 1978

ABSTRACT

Time series measurements of shallow-water waves and fluid-mud density variations, taken simultaneously with tide elevation and suspended sediment data, indicate that wave/fluid-mud interactions in the nearshore may be largely responsible for the present-day accumulation of fine-grained sediment on the open, unprotected coast of northeastern South America. Results of field experiments conducted along the central Surinam coast show that accumulations of fluid mud, which can be found up to 1.5 m thick on western flanks of migrating shore-attached mudbanks, affect incoming swell by changing their form from sinusoidal to solitary-like and by preventing wave breaking except for occasional spilling. As long-period swell (T = 12-16 sec) propagates over shallow banks of fluid mud, the wave height to water depth ratio remains nearly constant at 0.23; the steady decrease in wave height with shoaling water depth indicates that substantial amounts of wave energy are lost to a fluid-mud bottom even though breaking does not occur.

Evaluation of several mechanisms for the dissipation of wave energy reveals that attenuation of high-frequency waves (T < 3 sec) may be due to internal friction resulting from the extraordinarily high kinematic viscosity of muddy coastal waters. Additional energy is lost by viscous shear within a bottom boundary layer. Agreement with Keulegan's (1948) theory for energy dissipation for solitary waves on a smooth bottom is demonstrated when near-bottom boundary layer viscosities of 0.1 to 1.0 stoke are taken on a fluid-mud bottom. Additionally, unknown but large amounts of energy are lost as waves suspend soft, fluid mud.

A specially designed wave/fluid-mud pressure-sensing system, used successfully to obtain mean and fluctuating components of near-bottom or subbottom mud density variations during the passage of surface water waves, indicates that fluid-mud density fluctuates by 0.025 to 0.05 gm/cm^3 on a wave-by-wave basis. As each wave crest passes the sensing instrument, a cloud of sediment with particle concentration of approximately 50,000 mg/l is suspended instantly; rapid settling that follows is explained by the formation of a collapsing interface. Wave-by-wave sediment suspension is superimposed on a longer term suspension and deposition process that is related to stage of the tide. In water 1-5 m deep, suspended sediment concentrations increase beginning near time of mid-tide, reach a maximum at low water, then decrease steadily up to the following high water. Surface suspensate concentrations may exceed 3500 mg/l during this exchange process as 0.1-0.8 m of fluid mud is suspended in a 3-hour period of time near low water.

Utilizing the concept of wave-associated currents, it has been shown, in taking angle of wave approach, average observed concentration of sediment in suspension, and net drift as given by solitary wave theory, that volume transports of 3 to 70 x 10^6 m^3/yr can be explained by waves alone. These rates are perhaps 10-100 times higher than volume transport rates along typical sandy environments; high volume transport rates found by taking this approach do not require breaking waves and the concept of radiation stress and a nearshore circulation cell, as normally applied to sandy coasts. If a hypothesis of mud transport by solitary waves is accepted, then the continuous shoreward transport of suspended fluid mud, combined with the high rate of wave energy dissipation, explains in part the ability of muddy coasts to protect their shorelines.

ACKNOWLEDGMENTS

This research was performed under a contract between the Geography Programs, Office of Naval Research, Arlington, Virginia 22217, and Coastal Studies Institute, Louisiana State University. Considerable cooperation and field support were given by Drs. R. A. Cambridge and E. H. Dahlberg, Government Service for Mining and Geology, Ministry of Development, and Mr. A. M. Sutmuller and his staff, Hydraulics Research Division, Ministry of Public Works and Traffic, Surinam, South America.

I express appreciation to Drs. James M. Coleman, Barton R. Farthing, Harry H. Roberts, Joseph N. Suhayda, and Thomas Whelan, III, for critically reviewing the manuscript; to Drs. Stephen P. Murray and Wm. J. Wiseman, Jr., for helpful suggestions; to Dr. Gerald McHugh, Mr. Glenn Smith, and Ms. Mary White for aid in digitizing and computer programming; to Mrs. Rowena Hill for translation of an article; and to Mrs. Gerry Dunn for drafting. Mr. Rodney Fredericks designed and fabricated the wave/fluid-mud pressure-sensing system.

TABLE OF CONTENTS

LIST OF FIGURES

LIST OF TABLES

LIST OF SYMBOLS

A	Cross-sectional area, cm^2 or m^2
C	Wave celerity, cm/sec or m/sec
D	Grain diameter, cm
D_f	Rate of energy dissipation per unit area, dynes/sec/cm^2
E	Total wave energy per unit crest length, dynes
H	Wave height, cm or m
HW	High water
H_A, H_B, H_z	Depth references, cm or m
H_o	Initial wave height, cm or m
K_z	Pressure response factor, dimensionless ratio
L	Wave length, cm or m
LW	Low water
M	$(3H/h)^{1/2}$, dimensionless ratio
N	2H/h, dimensionless ratio; number of sample points
P	Wave power, ergs/cm/sec
Q	Total volume under a solitary wave crest per unit crest length, cm^2 or m^2
R_e	Reynolds number, dimensionless ratio
$R_T(\sigma)$	Power spectral density function
S	Salinity, parts per thousand (‰)
SWL	Still water level
T	Wave period, sec
Te	Temperature, °C
T_M	Mass transport, kg/yr
T_v	Volume transport, m^3/yr

$\bar{V}$	Volume transport velocity averaged from surface to bottom, cm/sec
W	Mudbank width, m or km
c	Suspended-sediment concentration, mg/l or gm/cm^3
cps	Cycles per sec, 1/sec
e	Voids ratio, dimensionless ratio
f	Frequency, 1/sec
g	Acceleration as a result of gravity, cm/sec^2 or m/sec^2
h	Water depth, cm or m
h_o	Initial water depth, cm or m
i	Square root of -1
k	Friction coefficient, dimensionless
m	Number of lags
n	Energy transmission ratio, dimensionless ratio
p	Wave pressure, dynes/cm^2
P_A, P_B	Depth-referenced pressure, dynes/cm^2
r^2	Coefficient of determination
$r_t(\tau)$	Autocorrelation function of $\eta(t)$
t	Time, sec
u	Horizontal particle velocity, cm/sec
u_b	Bottom horizontal particle velocity, cm/sec
v	Current velocity, cm/sec or m/sec
v_s	Particle settling velocity, cm/sec
w	Vertical particle velocity, cm/sec
x	Horizontal distance, cm or m
y	Elevation above the bottom, cm or m
z	Depth below SWL, cm or m

α	Angle of wave approach, degrees
β	Offshore slope
δ	Boundary layer thickness, cm
η	Wave profile elevation, cm or m
$\eta(t)$	Time series signal
μ	Dynamic viscosity, gm/cm/sec (poises)
ν	Kinematic viscosity, cm^2/sec (stokes)
ρ	Bulk density, gm/cm^3; water density, gm/cm^3
ρ_c	Deposited sediment concentration at a given bulk density, gm/cm^3 or kg/m^3
ρ_s	Sediment density, gm/cm^3
σ	Wave frequency, 1/sec
τ	Lag, sec
τ_b	Shear stress at the boundary, dynes/cm^2
ω	Radian frequency ($2\pi/T$), 1/sec

INTRODUCTION

A view traditionally held by geologists is that mud accumulates only in quiet, shallow basins; yet, the longest uninterrupted mud coast in the world spans 1600 km between the Amazon and Orinoco Rivers along the open, unprotected coast of South America, where deepwater wave statistics indicate high wave-energy levels. Many of the physical and geological processes that are important in maintaining this muddy environment take place in the nearshore region, where large accumulations of thixotropic gel, referred to as fluid mud or slingmud, are present. Recent studies have shown that the transportation of much of the sediment along this coast results from the northwestward migration of large shoreface-attached mudbanks, parts of which are composed of fluid mud (Delft Hydraulics Laboratory; 1962; Allersma, 1968; NEDECO, 1968). Further, the distribution of nearshore wave energy along the northeast coast of South America is controlled largely by these mudbanks, since accumulations of fluid mud have an attenuating effect on waves. Many of the unanswered questions about this muddy-coast environment concern the details of suspension, transport, and accumulation of fluid mud and the interaction between fluid mud and incoming waves. So that this interesting environment might be better understood, this investigation was undertaken in order to examine the process-form interactions between waves, fluid mud, and suspended sediment in the nearshore region.

Comparison among hydrologic and geologic surveys dated as early as 1670 indicated that large banks of fluid mud, originating near the mouth of the Amazon River, migrated to the northwest at an average rate of 1.5 km/yr (Allersma, 1968). Extensive field investigations in British Guiana (Delft Hydraulics Laboratory, 1962) and Surinam (NEDECO, 1968) affirmed the fact that these mudbanks, although exposed to wave forces from the Atlantic Ocean, were able to maintain their identity for decades. These studies further established, from visual observations, that waves were attenuated rapidly when moving over mudbanks, often to the point of disappearing before reaching shore. Although geomorphology of mudbanks, characteristics of coastal sediments, and general coastal oceanography, such as open shelf circulation, have been discussed in the literature (Zonneveld, 1954; Vann, 1959; Delft Hydraulics Laboratory, 1962; Eisma, 1967; Allersma, 1968; NEDECO, 1968; Gibbs, 1975, 1976), to date there is little published data on wave statistics and wave/fluid-mud interactions in the nearshore region of northeastern South America.

As early as 1968, the need for such wave data, other than from visual estimation, was noted by Allersma:

> ...it is felt that one or more series of observations with instruments, combined with a thorough analysis of the records, might reveal some facts that cannot be obtained from visual observations.

Specifically what is needed are continuous time series measurements of wave height, period, form, and angle of approach. Each time series should be of sufficient length to obtain the nearshore wave characteristics. Then, to answer specific questions concerning mudbank formation, wave attenuation and details of fluid-mud transport, additional data on nearshore currents, tide elevation, bottom changes, and suspended-sediment variations must be collected and analyzed.

In view of the above, the specific objectives of this study were: 1) to describe waves moving over a mobile, fluid-mud bottom by using electronic sensors and to examine the effect of this type of bottom and fluid-mud suspension on wave form and 2) to assess the role of waves in suspending and transporting fluid mud. These objectives were accomplished through field experiments conducted in four different hydrologic settings along the central Surinam coast. Much of the data on wave/fluid-mud interactions was collected by utilizing a wave/fluid-mud gage that was designed specifically for muddy environments. Time series records of waves and fluid-mud density changes were obtained simultaneously with tide height and suspended-sediment data. Fluid-mud samples were taken to determine mass physical properties of the bottom; fathometer profiles were run to determine mudbank morphology; and current profiles were taken over a tidal cycle to determine the nearshore residual current.

Previous Studies

Quantitative field data on process-form interactions in muddy-coast environments are lacking (McCave, 1972; Drake, 1976). The concepts for sediment suspension and transport by waves that were derived for low-turbidity waters and sandy bottoms, although abundantly present in the literature, cannot always be applied to highly turbid waters found along muddy coasts. Much of our knowledge of the interaction between waves, fluid mud, and suspended sediment stems from a few field studies, mainly by Dutch and Russian scientists, beginning in the early 1960s.

Delft Hydraulics Laboratory (1962), working on the coast of British Guiana, has undertaken perhaps the most ambitious field study yet conducted. An important conjecture with respect to sediment transport was that fluid mud could be transported en masse to the northwest by wave orbital scour. Large mudbanks spaced every 30-60 km along the coast were believed to propagate from southeast to northwest by the transport of fluid mud. Wave refraction diagrams for idealized mudbanks indicated that maximum convergence of wave energy occurred in mudbank "troughs." Normally a wave convergence would be expected on mudbank crests. It was hypothesized that a shoreward wave drift occurred in "troughs," whereas a return flow was present over mudbank "crests." Suspended-sediment concentration was found to increase with wave orbital velocity, leading to a regional distribution of suspended sediment that was related to wave activity.

NEDECO (1965), working in a similar environment in the Gulf of Thailand, found that in regions of fluid mud, waves were attenuated rapidly as a result of bottom friction. It was shown that sediment was brought into suspension by waves, then transported great distances by coastal currents.

Zenkovitch (1967), summarizing work by Russian scientists in the Gulf of Po Hai, reported that during wave disturbances bottom turbidity increased and a "creamy mass" was formed. Nearshore bottom water became most turbid when depths were "a few tens of cm" and waves impinged directly on banks of fluid mud. Waves and currents were found to remove complete layers of soft mud, presumably during storms, which later would be redeposited.

NEDECO (1968) conducted an extensive hydraulic investigation along the Surinam coast for navigational purposes. Fluid mud was found to damp wave motion and create conditions favorable for further sedimentation. The erosion of coastal muds was generally attributed to waves, but the large-scale mud transport, estimated at 2.5×10^8 m^3/yr, was believed to require a residual current farther offshore.

Nair (1976), elaborating on an earlier study by Moni (1970), documented the existence of mudbanks along the southwest coast of India that were nearly identical in morphology and sedimentology to those of northeast South America. These mudbanks, although formed only during monsoon seasons, served as a storehouse for littoral sediments and provided a buffer to

wave attack. It is interesting to note that boundaries of dangerously shoal accumulations of fluid mud in southwest India are usually delineated by visually noting the extent of the calming effect on incident waves.

A mathematical model to describe the effect of a fluid-mud bottom on shallow-water waves was given by Gade (1958) to explain the loss in wave energy over the "mud hole," a localized region of fluid mud off the central Louisiana coast (Morgan et al., 1953). Wave energy loss into a bottom that behaves as a viscous fluid was found to substantially reduce wave height; this energy loss greatly exceeded the dissipation over a rigid sand bottom. In a more general model where bottom sediments could not be considered as a viscous fluid, Gade (1959) found that energy dissipation took place as the bottom deformed elastically. In this case sediment structure was maintained and the bottom was not displaced laterally. Further work by Tubman and Suhayda (1976) has shown that Mississippi Delta muds respond to wave pressure forces elastically and thereby dissipate wave energy at a rate that is consistent with field measurements. Vertical bottom movements 1-2 cm high were found to dissipate wave energy at rates one or more orders of magnitude greater than those from percolation or normal frictonal effects.

In a series of laboratory experiments Lhermitte (1958; 1960) found that wave orbits could penetrate into fluid mud to substantial depths. With mud viscosities less than 20 centipoises, 2-m-high waves of 8-sec period were reported to cause oscillations down to 20-m depth. Later laboratory experiments performed by Migniot (1968) and Doyle (1973) verified that waves did impart orbital motions to fluid mud. At the "mudline," orbits were elliptical, whereas at the maximum depth of movement only horizontal motions were found. Analytical results presented by Bea et al. (1975) indicated that storm waves 20 m high and 14 sec in period could cause soil movement to 60 m below the mudline and a crest-to-trough "mudline wave" approximately 1.5 m high. These studies lead to the important conclusion that net drift resulting from non-closing wave orbits can cause mud transport in the direction of wave travel, provided offshore bottom slopes are gentle.

Despite the great number of investigations, certain problems concerning muddy-coast dynamics remain largely unsolved: 1) the origin of mudbank and fluid-mud deposits, 2) the attenuation of waves on a fluid-mud bottom, 3) the details of the mechanism of fluid-mud movement, and 4) the effect of fluid mud on coastal processes. In the ensuing paragraphs, parts of these questions will be answered.

FIELD AREA AND METHODS

Field experiments were conducted between 20 September and 8 October 1975 in the nearshore muddy waters of the central Surinam coast to obtain simultaneous data on waves, fluid mud, and suspended sediment during various stages of the tide. An instrument check and preliminary measurements were made in a similar environment along the Louisiana coast in November 1974.

The country of Surinam, situated midway between the Amazon and Orinoco Rivers, is representative of coastal conditions along the 1600-km coastline of northeastern South America. The warm, tropical climate is controlled by the northeast trade wind system. Although severe storms and hurricanes do not occur, alternating wet, windy and dry, calm periods are present throughout the year. September and October are typically dry months, and relatively calm sea conditions prevail. Beaches are composed of consolidated, prograded mudflats and are backed by mangrove swamps. Eight mudbanks, extending 5-10 km alongshore and 2-5 km offshore, front the coast every 30-60 km. Accumulations of fluid mud 1-2 m thick are present on western flanks of mudbanks and occasionally on mudbank crests. Pockets of sand and shell that often form between the rhythmic mudbanks comprise approximately 2

percent of the total volume of coastal sediments (Allersma, 1968).

Data were taken at four field sites, each representing a different hydrologic setting (Fig. 1): subaqueous mudbank (site 1); intertidal mudbank (site 2); Surinam River entrance (site 3); and area between mudbanks (site 4). Depending on stage of the tide, water depths ranged from 1 to 3 m on the subaqueous mudbank, 0 to 2 m on the intertidal mudbank, 5 to 8 m in the Surinam River entrance, and 4 to 7 m between mudbanks. Fluid mud, herein defined as a sediment-water mixture in which the sediment concentration is greater than 10,000 mg/l (Krone, 1962), was present on the subaqueous and intertidal mudbank sites and in the Surinam River entrance. Where fluid mud is present, the bottom is defined as the surface of the fluid mud layer, even though survey instruments may penetrate through it to more consolidated sediments (Odd and Owen, 1972, p. 183).

Time series data on wave characteristics (wave height, H; wave period, T) were recorded simultaneously with fluid-mud density changes on the subaqueous and intertidal mudbank sites (1 and 2). Wave data only were taken in the area between mudbanks where consolidated mud was present. These data were taken with a wave/fluid-mud pressure-sensing device designed and constructed at Coastal Studies Institute for use in muddy environments.

Two pressure transducers, fastened securely to 4-cm diameter pipe that was driven into the bottom, formed the sensing unit of this system. Figure 2 shows the position of pressure transducers relative to the fluid-mud bottom. On the first arrangement (site 1) transducer A was located near the level of low water (LW) and transducer B was placed 8 cm into the fluid mud; on the second arrangement (site 2) both transducers (A and B) were in the fluid mud. In most cases, surface-wave oscillations were recorded with transducer A and density changes in the fluid mud were recorded from the pressure differential between transducers A and B.

All wave and fluid-mud density data were recorded as analogue signals on a two-channel Gould Brush strip-chart recorder. Before reaching the recorder, signals were processed electronically to remove high-frequency noise and to enhance resolution. Details of this instrument and its use are given in Appendix I.

Water samples were taken at each field site in a 1-liter modified Van Dorn bottle at 0.5-1-hour intervals for suspended-sediment concentration and particle size determination. Surface samples were taken at the two field sites over the mudbank (sites 1 and 2); surface, mid-depth, and bottom samples were taken between mudbanks (site 4) and in the Surinam River entrance (site 3). A total of 82 samples was collected.

A tide record was obtained for the duration of the field experiments using a battery-powered pressure transducer water-level gage (fabricated at Coastal Studies Institute) that was fastened to a platform in the Surinam River entrance (Fig. 1). Two minutes of data were recorded continuously on a Rustrak recorder every 30 min. A 60-sec time constant filter removed high-frequency surface waves.

Current profiles were taken in the area between mudbanks (site 4) during a tidal cycle using a Bendix Q-15 meter (Bendix Environmental Sciences Division). Logistics problems precluded obtaining current data in the shoal water over banks of fluid mud.

A variety of background data was also obtained: salinity and temperature hydrocasts were taken at each field site every hour using a Beckmann RS5-3 inductive salinometer (Beckmann Instruments, Inc.); eight samples of fluid mud were taken over various parts of the mudbank and in the Surinam River entrance; fathometer profiles were run to determine mudbank morphology, offshore slope, and the extent of fluid mud; and an extensive aerial reconnaissance was undertaken to observe coastal landform variability.

All time series data (waves, currents, tide height, fluid-mud density) were digitized on a

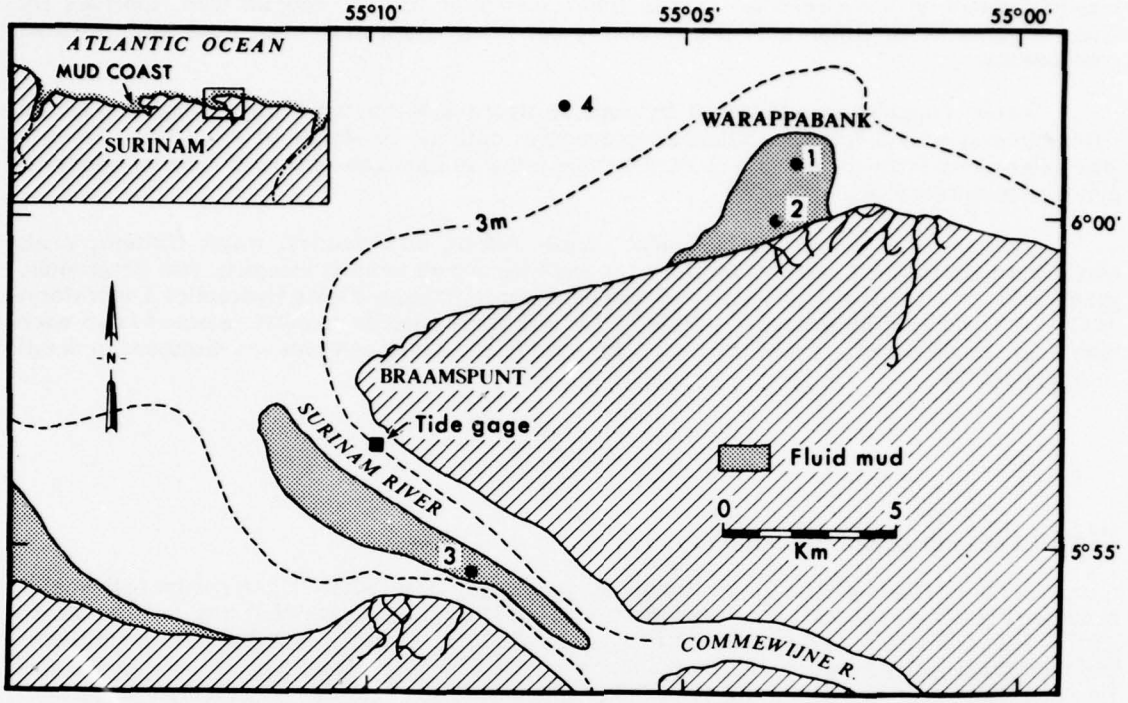

Figure 1. Index map to study area showing four field sites, central Surinam coast. The 3-m depth contour is referenced to mean low water.

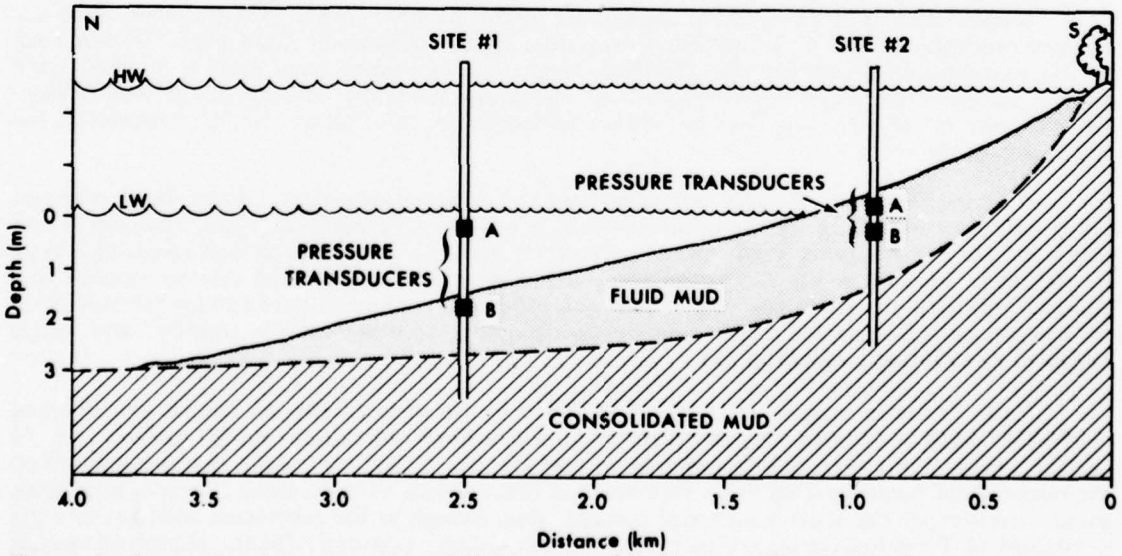

Figure 2. Generalized cross-section of fluid mud and field setup, Warappabank.

Calmagraphic III disc digitizing system (Calma Corporation). A standard stochastic analysis was performed on wave records using a Biomedical Time Series Program (see Appendix II). Current data were time and depth corrected, then separated into tidal and nontidal components.

Water samples were filtered through Millipore 0.45-micron filters using a pressure filtration system and following standard procedures outlined by Meade et al. (1975). Salinity was determined from the filtrate of each sample using an Elco Lab Line (Lab Line Instruments) conductive salinometer.

Mass physical properties (sediment concentration, bulk density, water content, voids ratio) were determined in the laboratory for each fluid-mud sample; viscosity was determined graphically on the basis of salinity and sediment concentration (Delft Hydraulics Laboratory, 1962). A standard pipette analysis (Folk, 1968) was performed on samples selected from each hydrologic environment. Laboratory methods used in the above analyses are discussed in detail in Appendix III.

RESULTS

Coastal Morphology and Hydrography

Accumulations of fluid mud appear as partial or "false bottom" returns on fathometer records (Fig. 3). Profiles taken over Warappabank (Fig. 1) indicate that the bottom slopes gently seaward at 0.00047 to 0.00073 (0°1'36" to 0°2'30"). Coastal mudbanks, each similar in form to Warappabank, were visible from the air at low tide along the Surinam coast and, together with the trough areas between mudbanks, displayed the spectacular pattern of erosion-accretion already well documented in the literature. Approximately 75 percent of the coastline is estimated to be stable or accreting. An example of shoreline progradation, as evidenced by stage of mangrove growth, is shown in Figure 4.

Warm, saline water is present along most of the Surinam coast. In situ temperature and salinity readings showed little variation over tidal cycles or between field sites. Within 5 km of the shoreline, in September and October, temperatures ranged from 28.7° C to 31.2°C and salinity ranged from 34.34 °/∞ to 35.86 °/∞. Discharge from the Surinam River (400 m^3/sec) turns rapidly to the west and does not affect temperature, salinity, or coastal processes at the field sites to the east.

Characteristics of the tide are important in fluid-mud dynamics. Water-level changes, taken continuously during the field experiments, are shown in Figure 5a. Major features of the tide are 1) a well-behaved, semi-diurnal periodicity and 2) a moderate to high range (3.2 m at spring tide). Because of the tide range and gentle bottom slope, fluid mud may be exposed to a distance offshore of more than 3 km during each low water. An estimated 25 km^2 of fluid mud on Warappabank is exposed twice daily; upon exposure, pore waters are expelled and initial stages of dewatering begin (Fig. 5b).

Tidal currents measured at site 4 in the area between mudbanks are rotary, opening clockwise, with maximum near-surface and near-bottom velocities of 55 cm/sec and 40 cm/sec, respectively (Fig. 6a). A residual current, setting to the northwest, is superimposed on the cyclic tidal currents (Fig. 6b). This residual flow, known as the Guiana Current, originates as an extension of the south equatorial current, then swings to the northwest and parallels the coastlines of French Guiana, Surinam, and British Guiana (Metcalf, 1968). Maximum speeds associated with this current are reported to be 100-200 cm/sec at a distance 30-40 km offshore. Maximum residual surface velocity at site 4, 5 km offshore, was 20 cm/sec.

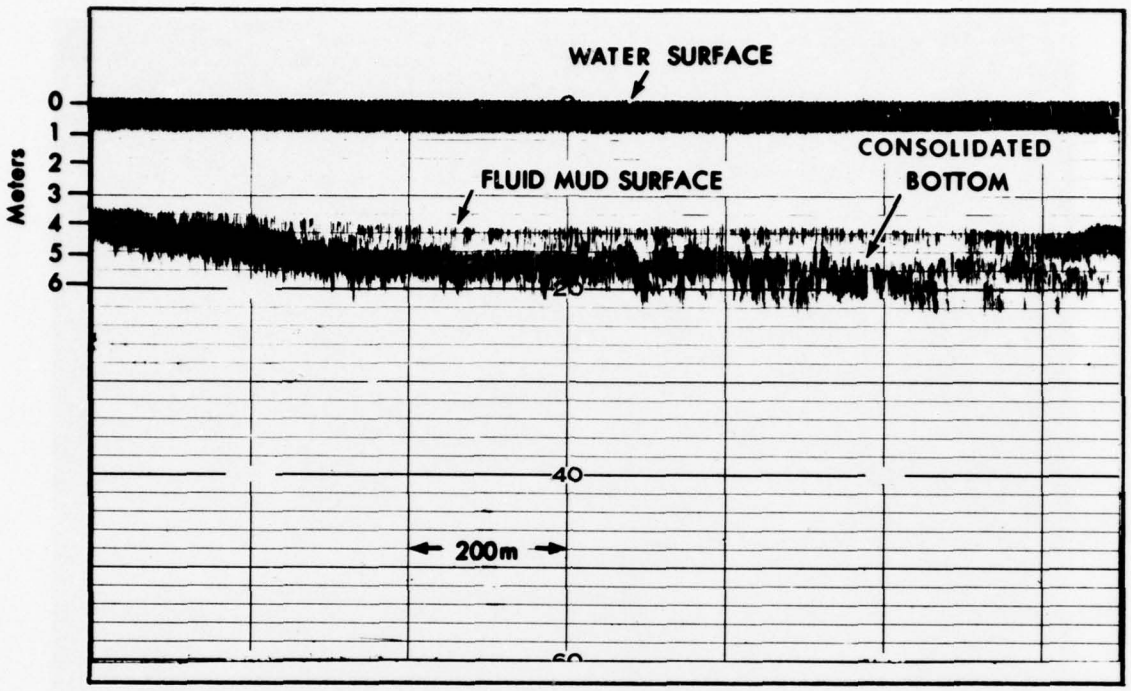

Figure 3. Fathometer profile of fluid-mud bottom, western edge of Warappabank.

Wave Characteristics

Examination of sixty-five 20-min wave records, taken over five sampling days, indicates that waves in the nearshore, with respect to wave form, are of two types: sinusoidal and solitary-like. In water 5-8 m deep between mudbanks, waves are generally sinusoidal, 0.5-1.0 m in height, and 12-15 sec in period. Assuming that linear wave theory applies, then

$$L = \frac{gT^2}{2\pi} \tanh\left(\frac{2\pi h}{L}\right) \qquad (1)$$

gives wave length, which, together with water depth in the ratio h/L, provides a classification for waves based on depth of water in which they travel. The observed h/L ratios ranged from 0.05 to 0.10, indicating that these are intermediate (transitional) water waves (Coastal Engineering Research Center, 1973).

A remarkable change in wave shape takes place when sinusoidal waves first propagate as shallow-water waves ($h/L < 0.05$) over a fluid-mud bottom. Wave records taken over mudbanks between HW + 2 hours and LW + 4 hours show that wave form closely approximates that for theoretical solitary waves. Isolated crests are separated by flat troughs lying at still-water level. Wave period is 12-16 sec and, in water 1-3 m deep, wave height is 0.1-0.5 m. Crests are steep and symmetrical, with lateral continuity, estimated from aerial reconnaissance to be more than 1 km (Fig. 7). Examples of the two types of wave forms are given in Figures 8a and b; the theoretical solitary wave form is given in Figure 8c.

Figure 4. Prograding coastline showing three levels of mangrove growth, eastern Surinam coast.

It is interesting to note that waves become more like true solitary waves in appearance as sediment concentration in water increases. Figure 9 shows a sequence of wave records, taken on the intertidal mudbank (site 2), that illustrates this effect. This series of wave records, spanning 3 hours, shows a marked change to solitary-like waves with flat troughs identically at SWL as surface suspended-sediment concentrations increase from 2750 to 20,000 mg/l. On intertidal portions of mudbanks, to be discussed later, the concentration of sediment is related to tide height, so that in many cases solitary wave appearance is also related to tide.

At LW, when banks of fluid mud are exposed, waves spill directly onto the fluid mud. During a rising tide there is no return flow associated with incoming waves; each wave simply advances farther toward shore and the water motion becomes borelike. On several occasions it was observed that, as waves impinged on a bank of fluid mud, wave energy was transferred from water to the fluid mud itself and a solitary-like wave propagated 600 m through fluid mud to the shoreline.

Field observations also revealed that, except during LW, when waves spilled onto banks of fluid mud, little wave breaking took place. Rather, wave height was continuously attenuated as waves traveled with a solitary-like wave form over 1-3 km. Most waves do not reach the shoreline. A plot of wave height versus water depth for 25 wave records taken over the mudbanks indicates that over fluid mud waves decrease in height linearly with decreasing

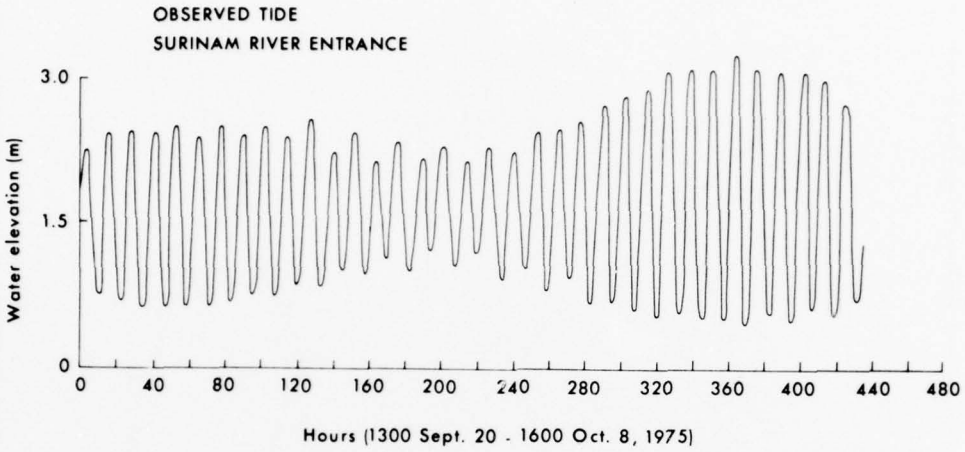

Figure 5a. Tide record in the Surinam River entrance during the period of investigation. This gage was not tied in to a geodetic or leveling net.

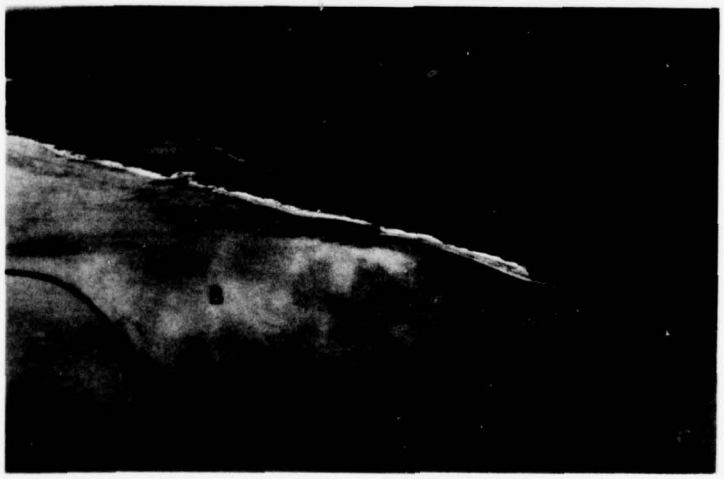

Figure 5b. Photograph illustrating mud exposure at low-water spring tide in the vicinity of field sites 1 and 2: (A) muddy coastal water, (B) bank of exposed fluid mud, and (C) newly accreted wedge of fluid mud forming a coastal mudflat that is being actively colonized by mangroves.

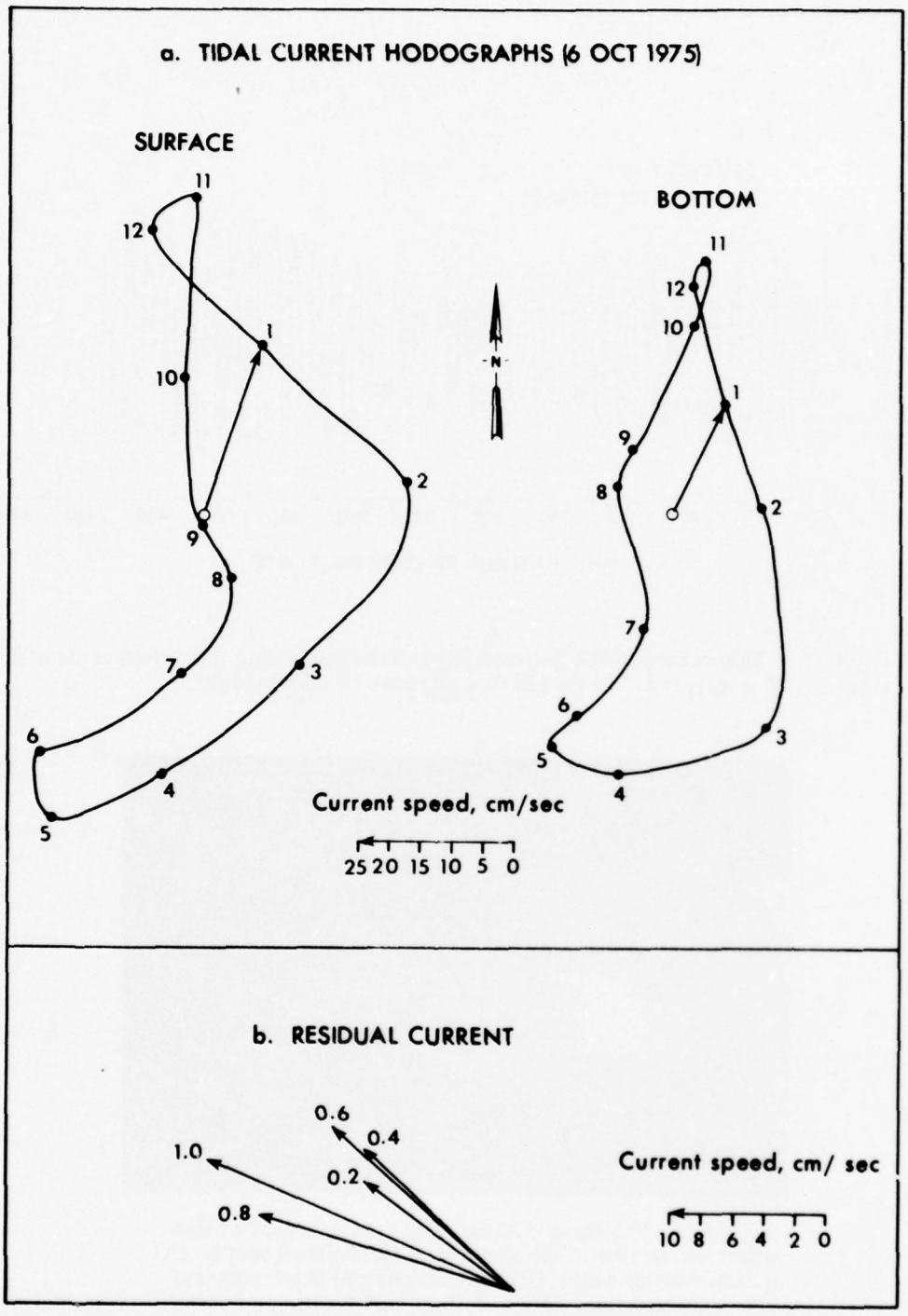

Figure 6. Tidal current hodographs, surface and bottom (a), and vertical profile of relative depth (0.2 bottom; 1.0 surface) residual current vectors (b), in the area between mudbanks (site 4).

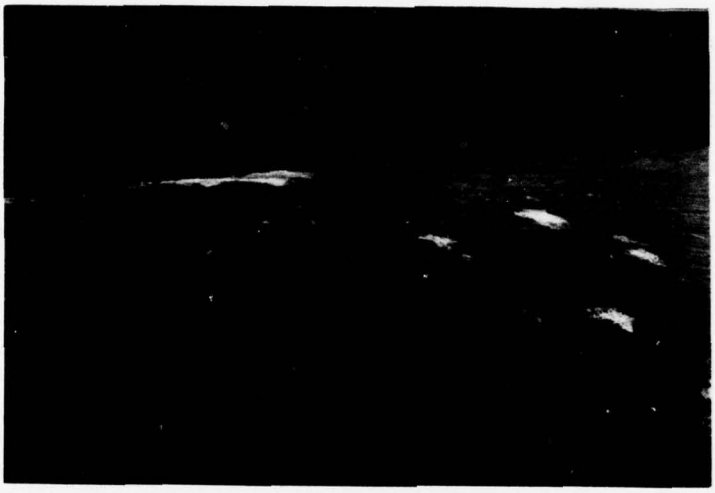

Figure 7. Solitary-like waves from an altitude of 250 m. Note overall crestal continuity (center) and disappearance of waves in fluid mud (upper right).

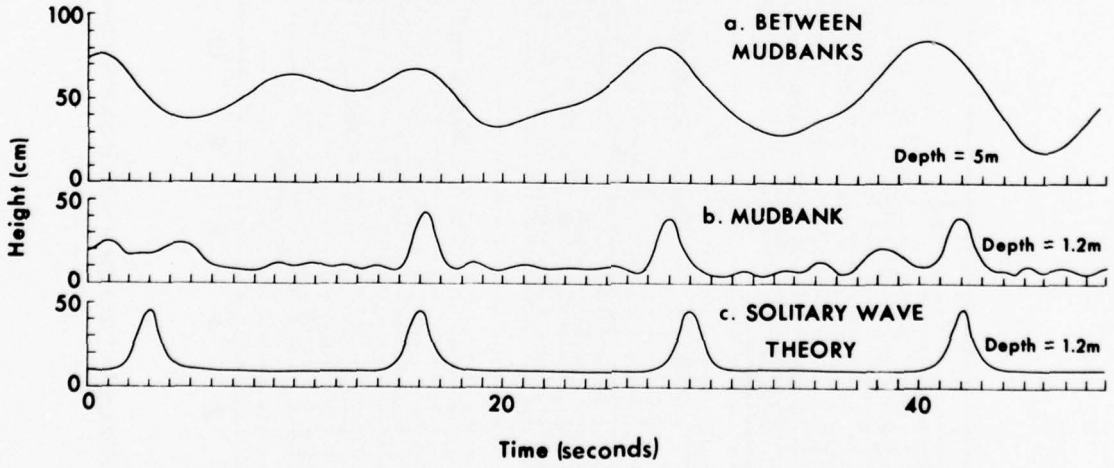

Figure 8. Sinusoidal wave form in area between mudbanks (a), solitary-like wave form over subaqueous mudbank (b), and wave form as given by solitary wave theory (c).

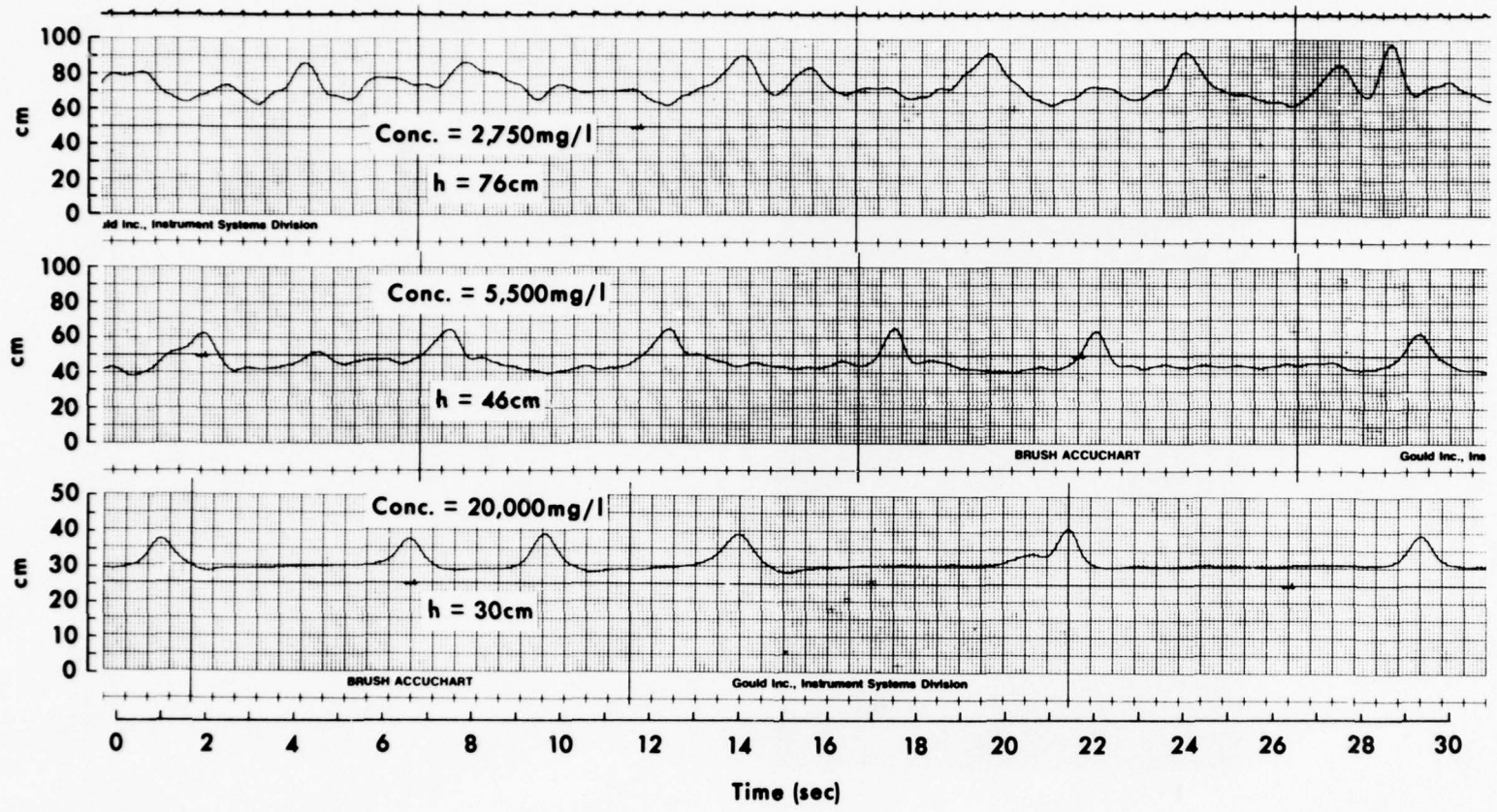

Figure 9. Change in wave form with increasing sediment concentration and decreasing water depth, intertidal mudbank.

water depth (Fig. 10). An interesting feature of this figure is that the slope of the least squares best fit line corresponds to an H/h of 0.23; 96 percent of the H/h ratios measured were less than 0.33. The H/h ratio at which waves break, from solitary wave theory, was shown by McCowan (1894) to be 0.78. Laboratory and field measurements over rigid bottoms show H/h ranges between 0.73 and 1.03. Thus as solitary-like waves advance into shoaling water over a fluid-mud bottom, they appear to have, on the average, an H/h ratio considerably less than the value that might be expected from solitary wave theory or from measurements over sandy bottoms. This indicates high levels of wave-energy dissipation.

Additional information on shallow-water solitary-like waves can be obtained from the wave spectrum. Typical spectra of waves at site 1 (subaqueous mudbank) are given in Figure 11. Three features are noteworthy in the spectra. First, these spectra contain a low-frequency energy peak in the infragravity range, 33-80 sec (0.03-0.0125 cps). Next, there is a wide distribution of wave energy over all frequencies; on many of the spectra examined these secondary energy peaks occur at harmonic frequencies. Third, the decay rate of secondary peaks is roughly exponential.

The effects of a fluid-mud bottom on waves in shallow water, as manifested in the wave spectrum, can be observed in Figure 12a-d. This figure reveals some interesting points. A "characteristic" energy peak, encompassing a narrow range of frequencies, is present in the spectrum of waves from the area between mudbanks (Fig. 12a). Only 1 percent of the wave energy appears to be contained in frequencies higher than 0.2 cps, although the natural filtering effect of the pressure transducer, placed 4 m below the surface in this instance, accounts for some of the apparent high-frequency loss. The next two spectra (Fig.12b-c) are of waves moving across identical bottom slopes (β = 0.0005), each in 1.3-m water depth, but over different bottom consistencies. Waves on the Louisiana coast, where the mud is more consolidated, have a sinusoidal form and relatively narrow range of frequencies, whereas those on the Surinam coast are solitary-like and have an apparently wide distribution of energy. Some similarity in the distribution of wave energy to a wave spectrum generated from perfect solitary waves is shown in Figure 12d. The difference in vertical scales should be noted.

Although the peak energy density associated with the waves between mudbanks is more than an order of magnitude greater (approximately 25x) than for waves over the mudbanks, root mean square height is only 1.5 times greater, whereas total wave energy is 3 times greater.

Angle of wave approach at the shoreline, as determined from visual estimates in the field and from measurements on aerial photographs, ranges from 3° to 8° in shallow water over mudbanks and 5° to 10° between mudbanks.

Suspended Sediment

The highest overall suspended-sediment concentrations and the greatest variability in concentration occur over the mudbanks, whereas the lowest and least variable concentrations occur between mudbanks. These results, plus data from the Surinam River entrance, are given in summary form in Table 1.

Figure 13a-d shows details of suspended-sediment change with stage of the tide. The major features of concentration change over the subaqueous mudbank are a rapid increase at mid-tide, peak at low water, then steady decrease to the following high tide. A concentration change of more than two orders of magnitude takes place in surface water during each tidal cycle. On the intertidal portion of the mudbank, concentration changes are even more pronounced. Because sampling began precisely at LW, when fluid mud was exposed, the initial concentration of approximately 200,000 mg/l shown in Figure 13b is that of fluid mud rather than of suspended sediment. As water level rose, these suspended-sediment concentrations

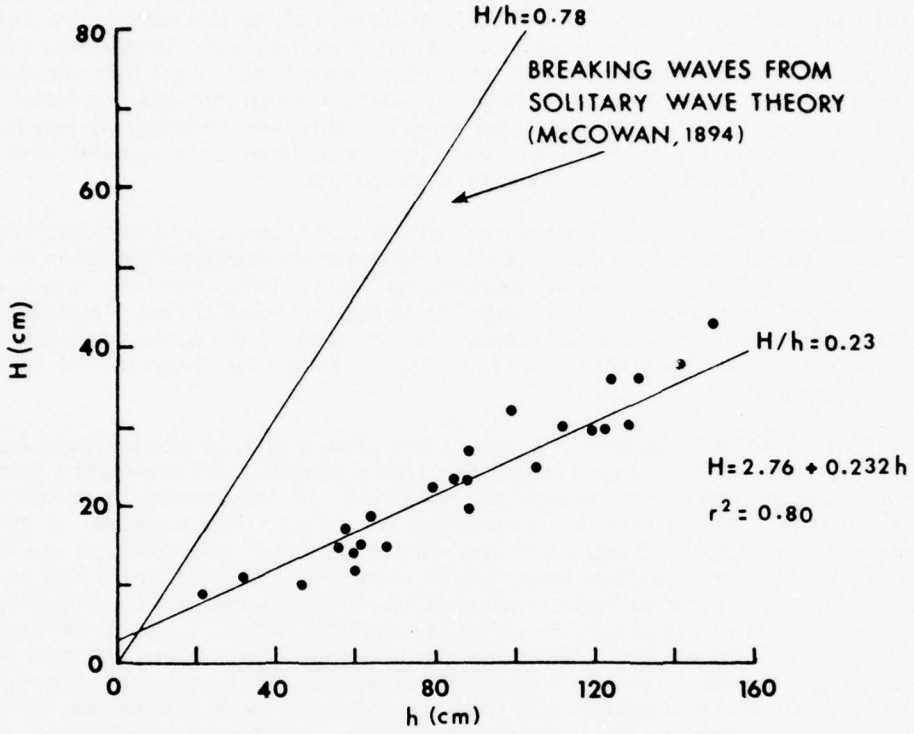

Figure 10. Wave height versus water depth for twenty-five 20-min wave records taken at the subaqueous and intertidal mudbank field sites.

decreased. The relationship between tide height and concentration for all samples collected over the mudbank is given in Figure 14.

In contrast to the sites described above, no trend can be observed with stage of the tide in the region between mudbanks (Fig. 13d), and concentrations remain 1-2 orders of magnitude lower than elsewhere. Regardless of stage of tide, concentrations increase with depth.

In the Surinam River entrance, a region also influenced by fluid mud, sufficient data were not available to determine the presence of a well-defined trend. As before, suspended-sediment concentrations increase with depth, and in the region near the bottom, fluid mud persisted at all stages of the tide.

Fluid-Mud Dynamics

Table 2 gives characteristic values of bulk density, water content, voids ratio, and viscosity for fluid mud in several locations along the coast and one location in the Surinam River. Bulk density is always highest in fluid mud that is undergoing dewatering, as, for example, on the intertidal mudbanks, which are exposed 1-3 hours during each LW. Minimum bulk density was observed in fluid mud in the Surinam River channel, where strong currents prevent consolidation. It should be noted that considerable variation in these values within a given fluid-mud body is possible since densities increase near the base of the fluid-mud deposit. Water content and bulk density are inversely related, but in a strongly nonlinear fashion.

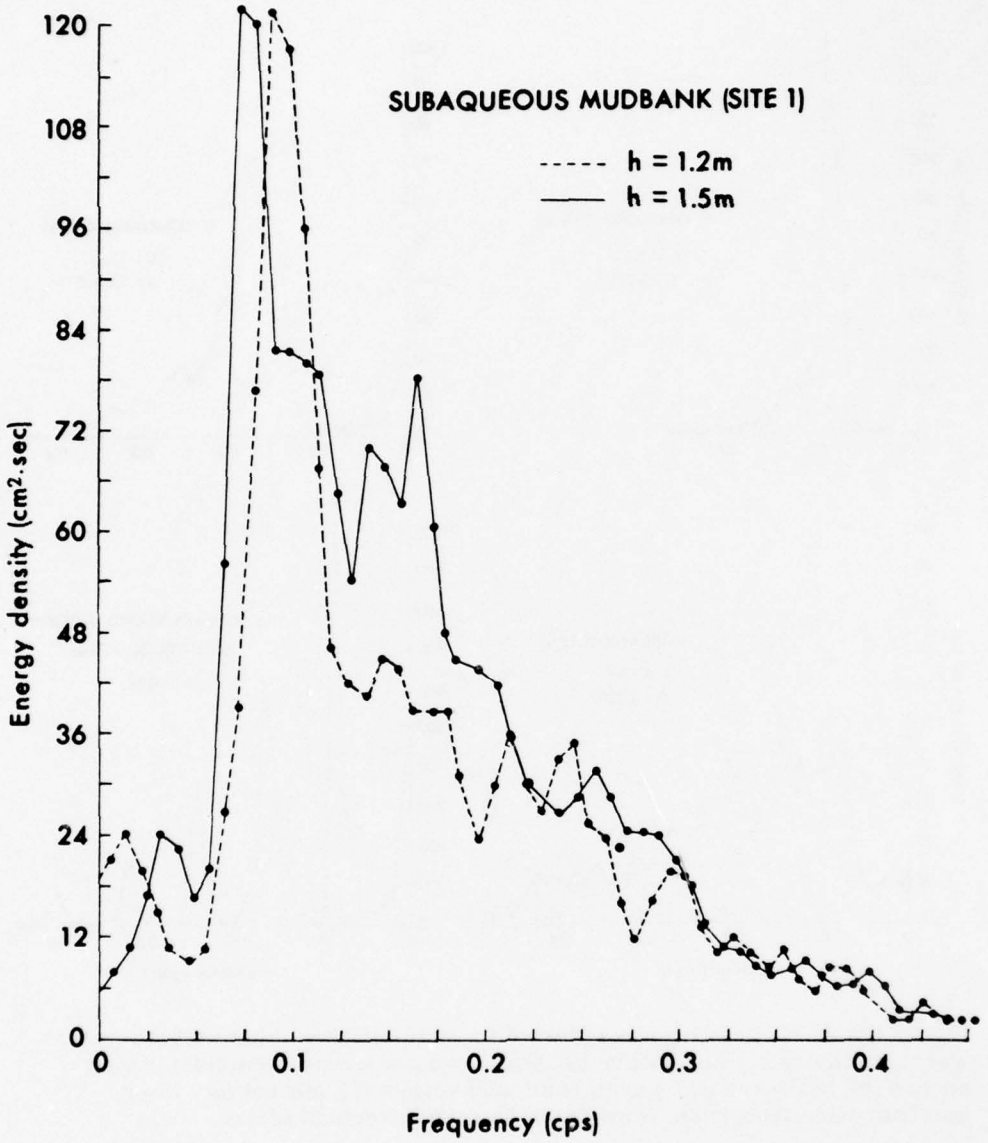

Figure 11. Typical wave spectra from the subaqueous mudbank field site.

Viscosity increases exponentially with bulk density and spans over four orders of magnitude within the range of fluid-mud concentrations observed in this study.

Typical particle-size distributions for coastal and river muds are given in Figure 15. Median diameter of particles in unpeptized form is 0.5 to 1.0 micron, although it is likely that particle aggregates many times larger can exist. Less than 1 percent of individual particles is coarser than clay size, and the brown, fine muds along the Surinam coast are remarkably uniform in size.

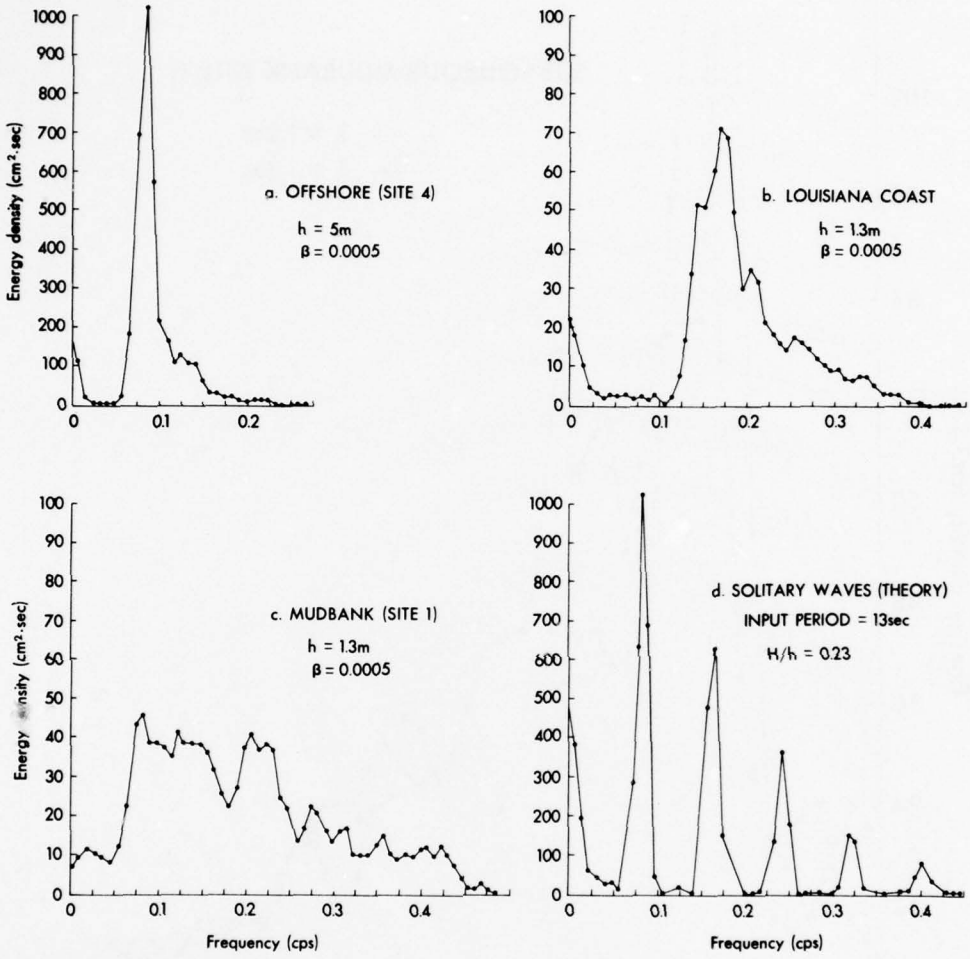

Figure 12a-d. Contrasting wave spectra for mud bottoms. Intermediate-water waves, consolidated mud bottom (a), shallow-water waves, consolidated mud bottom (b), shallow-water waves, fluid-mud bottom (c), and solitary wave spectrum from theory (d). Note the difference in vertical scales.

Observations made on a bank of fluid mud at LW indicate several interesting features. Within an hour after fluid mud is exposed on an ebbing tide, a layer (1-3 cm thick) of very clear water appears presumably owing to the initial stages of dewatering. This water gives the fluid mud a glassy appearance when observed from the air (Fig. 5b). Under shear from a northeast wind, estimated at 15 kn, particles from the surface of the fluid mud are picked up and carried in suspension within this water layer as it begins to flow. Bottleneck flowage and tensional cracks that have vertical walls several centimeters thick provide evidence that the entire bank of fluid mud moves when it is exposed at low tide. The thixotropic character of the fluid mud was revealed when small mass movement failures were gently disturbed; the fluid mud lost its

Table 1

Maximum and Minimum Suspended-Sediment Concentrations at Four Field Sites, Central Surinam Coast

Hydrologic Setting	Sampling Depth	Concentration		Range in Water Depth (m)
		Maximum	Minimum	
		(10^2 mg/l)		
Subaqueous Mudbank (Site 1)	Surface	37.49	0.34	1-3
Intertidal Mudbank (Site 2)	Surface	2222.85*	26.57	0-2
Surinam River Entrance (Site 3)	Surface	11.98	0.49	5-8
	Mid-depth	33.02	0.64	
	Bottom	303.62*	240.02*	
Between Mudbanks (Site 4)	Surface	0.27	0.14	4-7
	Mid-depth	0.82	0.16	
	Bottom	1.22	0.92	

*"Suspensions" with concentrations greater than 100 x 10^2 mg/l are generally referred to as fluid mud (see Krone, 1962). Maximum values at site 2 correspond to samples from mudbank surface exposed at low tide.

internal strength, which was originally sufficient to maintain a vertical wall, and the tensional features collapsed instantly.

Fluid mud responds rapidly to the passage of waves. Figure 16 shows examples of density changes that occur on the subaqueous mudbank in a 40-cm interval near bottom For reasons discussed in Appendix I, two scales are present on each differential density record, one for long-term density changes and the other for wave-by-wave changes. As each wave passes. fluid mud is suspended and a density change of 0.025 to 0.05 gm/cm^3 takes place. Careful examination of these records reveals the important fact that maximum density precedes the wave crest by 0.5-1.0 sec. At the instant of crest passage, density is approximately one-half its peak value, and 1-2 sec after the crest passes, near-bottom density reaches its lowest value. The magnitude of wave-by-wave density variation decreases after 1255 hours, even though the surface waves remain nearly the same height. It should be noted that values obtained from this figure are for average density changes between pressure transducers. Absolute near-bottom density could not be obtained, but is estimated to range from 1.16 gm/cm^3 at transducer B to 1.03 gm/cm^3 at transducer A; a sharp gradient occurs in the region 10-30 cm above transducer B.

These wave-by-wave changes are superimposed on a longer term differential density variation that is related to tide. Beginning at 1115 hours, between time of mid-tide and LW, two changes take place. First, a slight increase in differential density, 0.012 gm/cm^3, occurs between 1115 and 1245 hours. Next, a rapid decrease of 0.040 gm/cm^3 takes place between 1245 and 1255 hours, the approximate time of LW. By the time of termination of the experiment, at 1445 hours, differential density was reduced an additional 0.020 gm/cm^3.

Figure 17 shows density changes, beginning at LW, in the upper 0.5 m of fluid mud on the intertidal mudbank. Five time series sections. each approximately 20 min long, show that

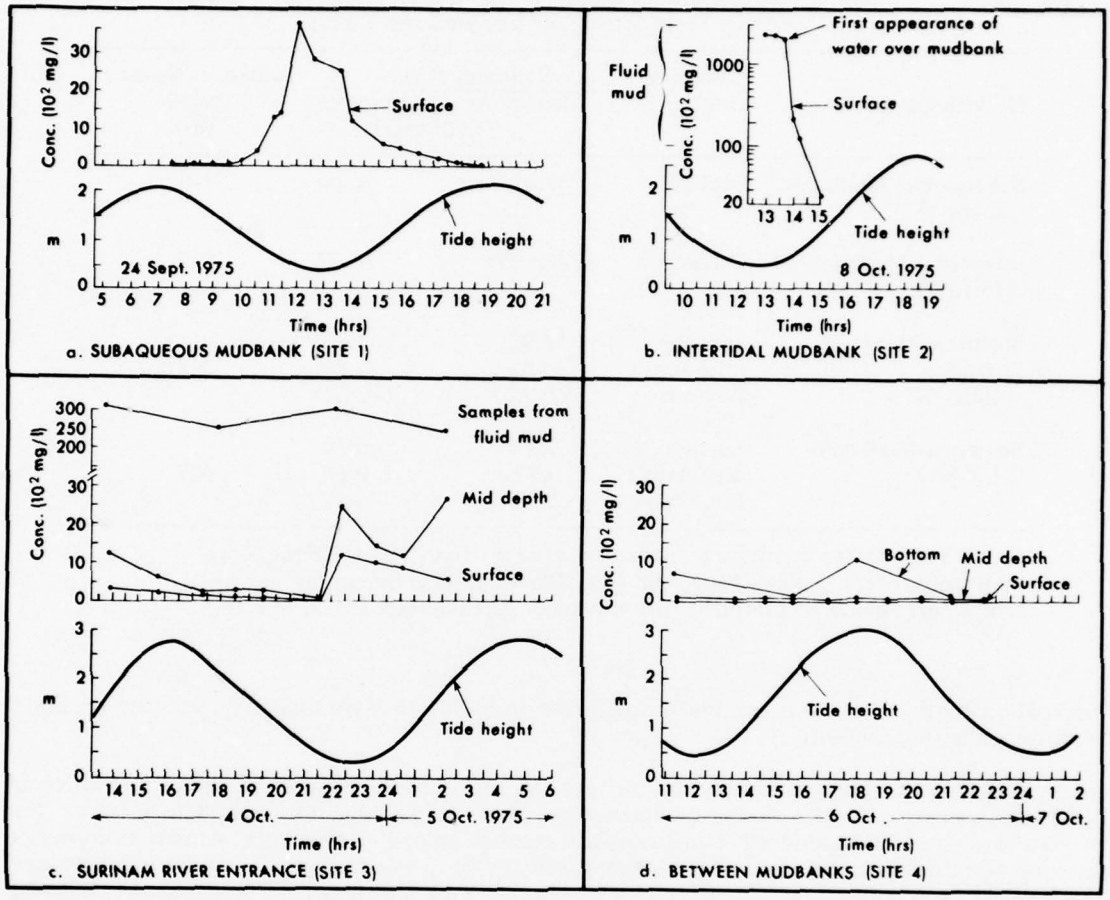

Figure 13a-d. Suspended-sediment variations at four field sites. Subaqueous mudbank (a); intertidal mudbank (b); Surinam River entrance (c); area between mudbanks (d).

bulk density decreased from approximately 1.16 gm/cm^3 to 1.05 gm/cm^3 over a 3-hour period as water level rose. An important feature of these data is that, although water did not begin to cover the fluid mud at the field site until 1335 hours, a measurable change in average fluid-mud density had occurred prior to this time. Considerable density variation in the frequency range ≤ 5 min is evident; however, regression analysis shows that each section of time series has a statistically significant slope.

DISCUSSION

Solitary Waves in a Viscous Fluid

The effect of a fluid-mud bottom on waves has been noted for more than two centuries (Bristow, 1938). Although waves in shallow water are often considered as having some features

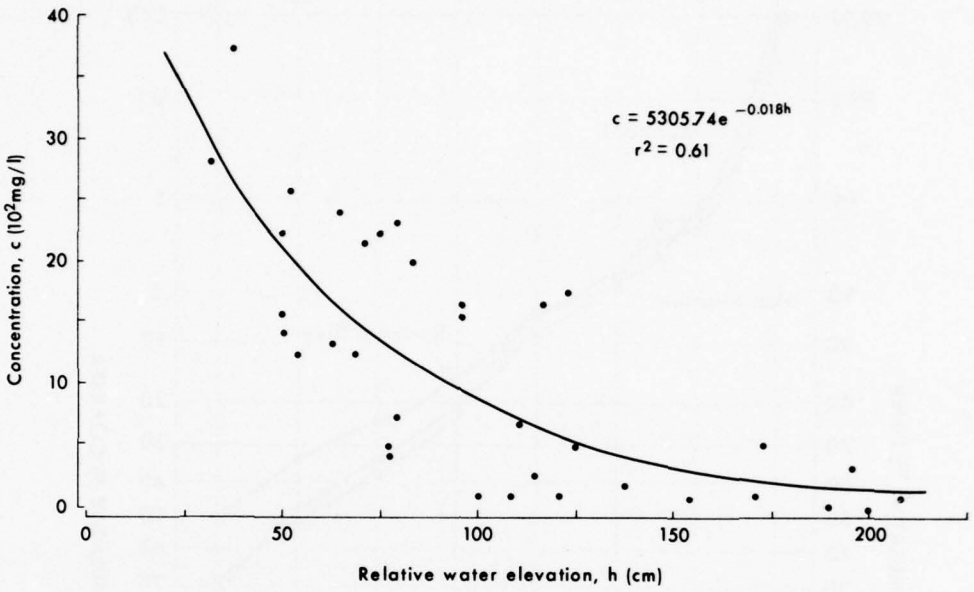

Figure 14. Suspended-sediment concentration versus water elevation due to stage of the tide for all samples taken over the mudbank.

Table 2

Physical Properties of Fluid Mud, Surinam Coast

Location	Bulk Density (gm/cm^3)	Water Content (%)	Voids Ratio	Viscosity (cm^2/sec)
Mudbank exposed at LW (Site 2)	1.172	380	10.1	210
Mudbank covered by 2 m of water (Site 1)	1.140	490	13.0	75
Mudbank-water interface	1.052	2030	53.8	0.06
Surinam River entrance	1.036	4350	115.3	0.02

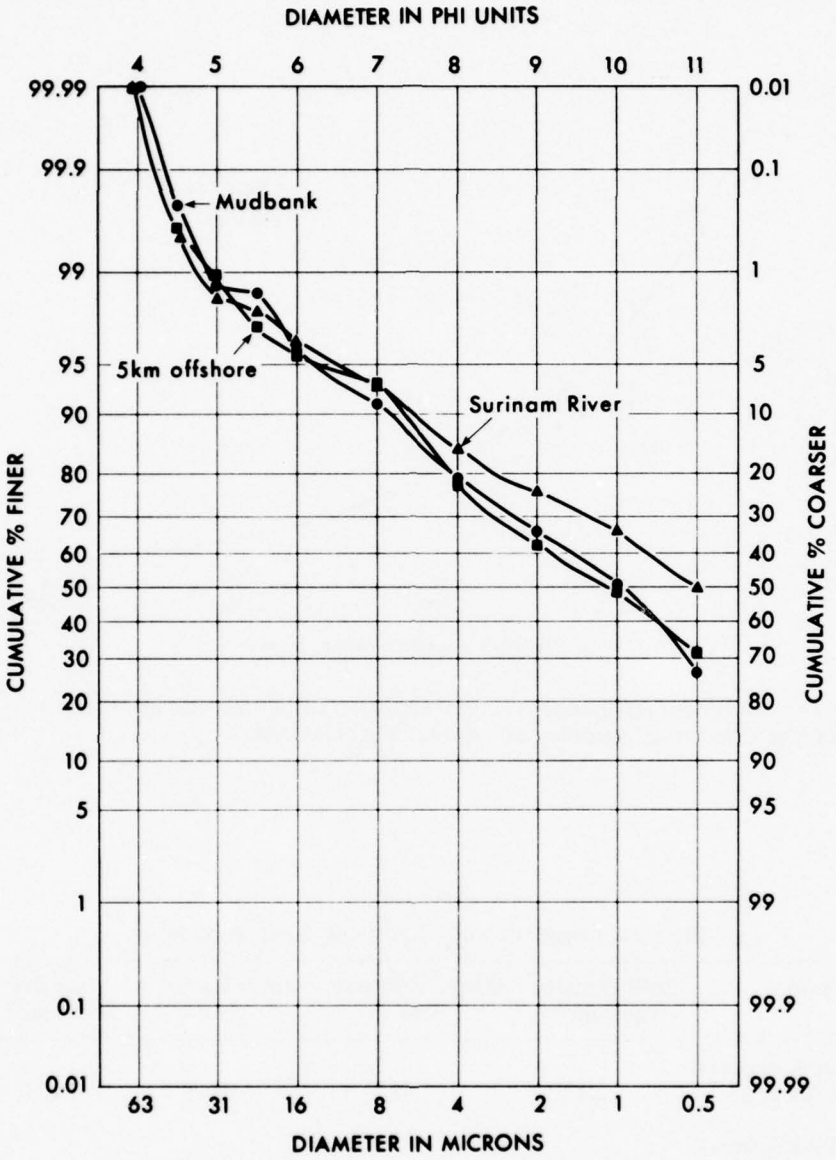

Figure 15. Typical particle-size distributions, central Surinam coast.

of a solitary wave, this study shows for the first time that the form of these waves moving over fluid mud is remarkably close to that given by solitary-wave theory.

Taking water surface elevation in the time-space domain to be

$$\eta = H \operatorname{sech}^2 \left[\sqrt{\frac{3}{4}\frac{H}{h^3}} (x - Ct) \right] \qquad (2)$$

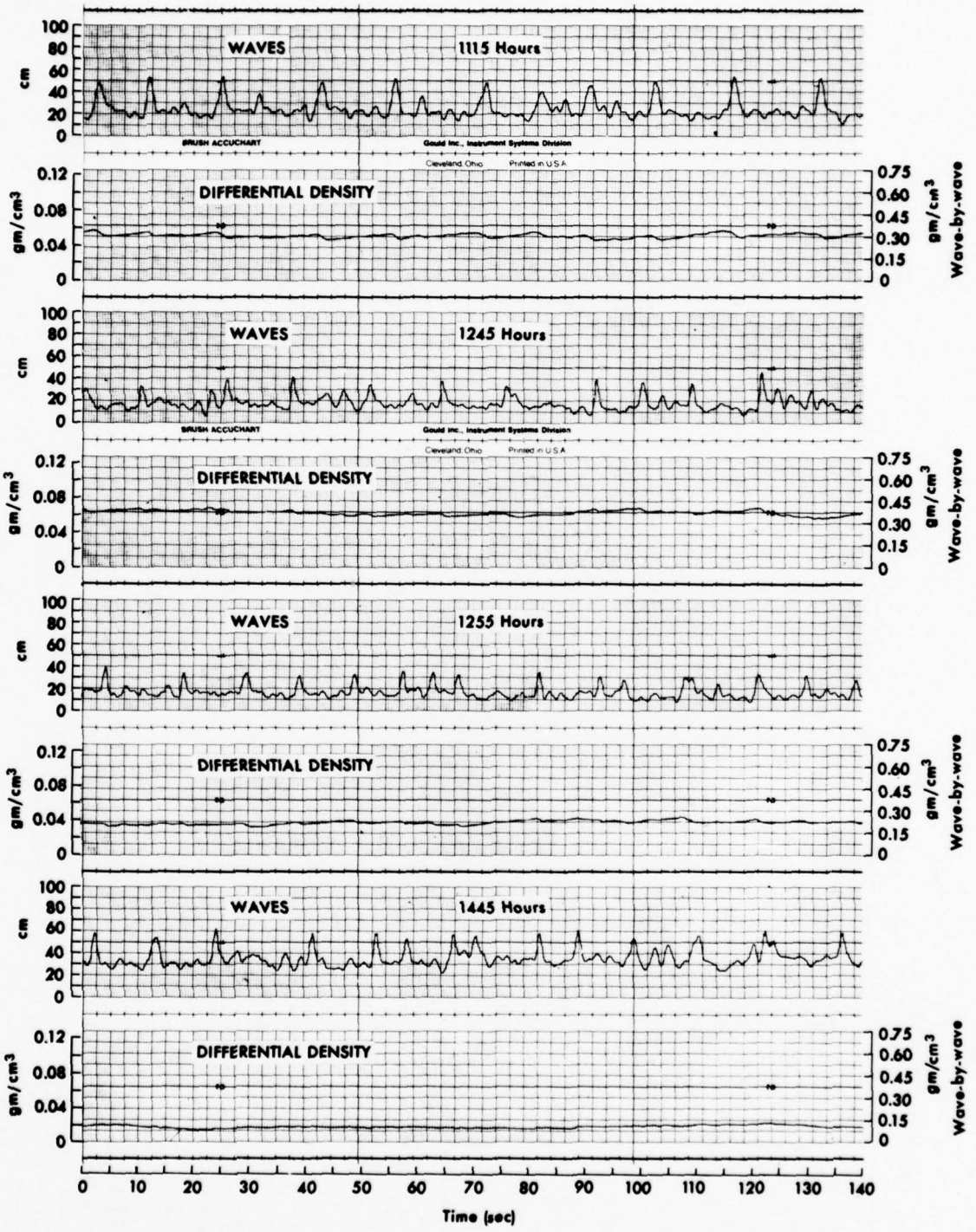

Figure 16. Variations in near-bottom fluid-mud density, subaqueous mudbank (site 1). Data were taken between HW + 4.5 hours and LW + 2 hours.

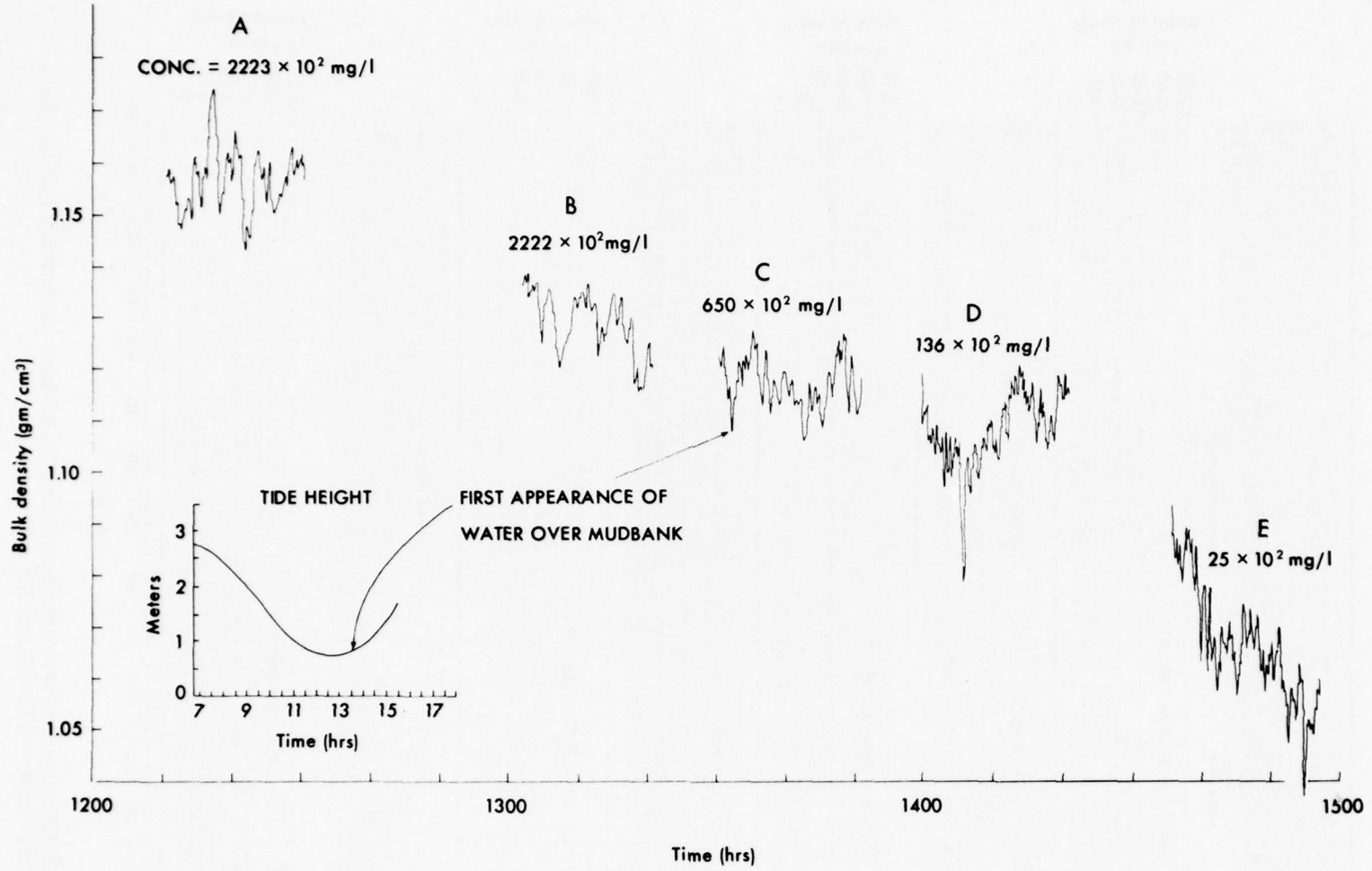

Figure 17. Time series of bulk density changes in upper 0.5 m of fluid mud, beginning at LW. Values above each time series section (A-E) represent surface suspended-sediment concentration.

a solitary wave is described that has as its major features a symmetrical crest entirely over SWL and a trough that corresponds exactly to the level of still water. This wave, unlike waves given by Airy, Stokes, and Cnoidal wave theories, is specified completely by wave height and water depth.

The primary difference between waves shown in Figures 8b and 9 and waves given by equation 2 is in the troughs. An average trough level is, in many cases over the mudbank, very close to SWL, but high-frequency, low-amplitude waves are present between crests and the troughs are seldom completely flat. Dispersive waves in trough regions make it difficult to form a true solitary wave in nature (Coastal Engineering Research Center, 1973, p. 2.59).

The disappearance of these dispersive waves with increasing sediment concentration (Fig. 9) is an excellent example of the filtering effect of high sediment suspension in water and offers evidence that a fluid-mud bottom and high sediment concentrations in the water column do indeed lead to wave transformation to solitary-like waves. It can be argued that waves in the areas between mudbanks, upon reaching the same depth of water as solitary-like waves over mudbanks, would have similar characteristics. Two lines of evidence suggest that this is not the case. First, observations made from a boat traveling parallel to bottom contours revealed a sharp change in wave form when it crossed onto a region of fluid-mud bottom. It is estimated that boundaries of fluid mud can be delineated within 10 m simply by visual observation. Second, shallow-water wave spectra from Surinam and Louisiana differ considerably, even though waves from both regions travel for at least 30 km over a mud bottom with identical bottom slope.

A rigorous evaluation of the effect of fluid mud on wave characteristics is a formidable problem that, as far as the author is aware, has not been undertaken. Results from this study revealed at least two factors that complicate such an evaluation. First, the bottom is not rigid but is highly mobile and, relative to a fixed consolidated mud bottom beneath, will change position as fluid mud is suspended. Second, the fluid-mud bottom undergoes density changes that display frequencies from those of waves (~10-15 sec) to that of the tide (~12.4 hr). Viscosity of water near bottom is not constant inasmuch as fluid mud is periodically suspended into the water. Even lacking the density and viscosity changes attributed to waves, the near-bottom situation is complicated because a sharp density gradient occurs in a bottom layer estimated to be 10-30 cm thick.

Solitary wave theory was derived under the simplification of an inviscid fluid and the boundary condition of a rigid bottom. As mentioned above, neither of these assumptions holds true for waves over mudbanks. Equations that govern wave motion in general neglect viscous forces, thus giving a solution with non-zero velocity at the bottom. Oscillatory waves on an impermeable sandy bottom have a no-slip condition imposed at the boundary so that the effects of viscosity are felt only in a boundary layer in the immediate vicinity of the bottom (~1 cm or less). Therefore, viscous forces are usually negligible, and this explains the success of wave theories that were developed for inviscid fluids (Madsen, 1976).

One effect of high viscosity and a fluid-mud boundary such as exists in Surinam may be to enlarge the boundary layer. Given boundary layer thickness under a periodic wave

$$\delta = 5\left(\frac{2\nu}{\omega}\right)^{1/2} \qquad (3)$$

where ν is kinematic viscosity, viscosities in the range of 1-10 stokes for 15-sec waves will increase the boundary layer from 1 to perhaps 10-30 cm. In fact, the entire fluid-mud deposit may act as a boundary layer. NEDECO (1965) has suggested that where thick accumulations of fluid mud are present fluid flow in the near-bottom boundary layer may be laminar and may have Reynolds numbers of about 250. Under laboratory conditions, estimated boundary layer thickness beneath solitary waves is given by Ippen et al. (1955) as

$$\delta = \frac{12.7}{\sqrt{R_e}} \left(\frac{H}{h}\right)^{1/2} H \qquad (4)$$

where the wave Reynolds number,

$$R_e = \frac{1.54 \sqrt{gH}\, H}{\nu} \quad . \qquad (5)$$

Again taking viscosities in the range of 1-10 stokes, $R_e < 10^3$ and $\delta > 10$ cm are attainable. Low R_e and boundary-layer growth resulting from the predominating viscous forces are associated with high rates of energy dissipation.

The most important effect of increased viscosity in the water column is wave height attenuation. Ordinarily, waves increase in height with decreasing depth up to the point of breaking. In the general case for linear wave theory, wave energy flux, P = ECn, is assumed to remain constant from deep to shallow water so that

$$P = (ECn)_o = ECn = \text{CONSTANT} \qquad (6)$$

where the subscript "o" represents initial conditions and the energy transmission ratio, n, is defined as $1/2 \leq n \leq 1$, depending on water depth.

Now, considering solitary waves in shallow water where the energy transmission ratio is unity

$$C_o E_o = CD \quad . \qquad (7)$$

In this case E is given as

$$E = \frac{8}{3\sqrt{3}} \rho g \left(\frac{H}{h}\right)^{3/2} h^3 \qquad (8)$$

and C, given to a close approximation by Boussinesq (1872), is

$$C = \sqrt{gh\,(1+H/h)} = \sqrt{g(H+h)} \quad . \qquad (9)$$

Substituting equations 8 and 9 into equation 7 yields

$$\frac{H}{H_o} = \frac{h_o}{h} \left[\frac{h_o}{h} \left(\frac{1+H_o/h_o}{1+h/h}\right)\right]^{1/3} \quad . \qquad (10)$$

This is shown by Ippen and Kulin (1955) to be nearly equivalent to

$$\frac{H}{H_o} = \left(\frac{h_o}{h}\right)^{4/3} \quad . \qquad (11)$$

Thus, on the basis of constant energy considerations, for solitary waves an increase in wave height would be expected with decreasing water depth. Laboratory studies have verified the form of equation 11 for predicting wave height, although wave tank experiments show that actual heights are less than predicted by this equation (Ippen and Kulin, 1955). However, field data from the present study, given in Figure 10, indicate that over fluid mud just the opposite occurs.

That the discrepancy between actual and predicted wave heights for a given set of conditions is substantial is shown in Figure 18. For example, according to solitary-wave theory, a wave 100 cm high at the seaward edge of fluid mud in a water depth of 5 m would attain a height of 200 cm after traveling to a depth of only 3 m. Shortly after that, the wave would break. In reality a wave 100 cm high follows the H/h = 0.23 line and at 3-m depth is 60 cm high, less than 1/3 the predicted height. This wave would probably not break, but would continue to decrease in height up to the shoreline. Whereas Ippen et al. (1955) found that damped solitary waves maintain their original volume by becoming flatter in profile, no such change in wave shape was noted in this study.

Wave energy loss or wave damping, as manifested in height attenuation, can be caused by many factors: bottom percolation; free surface dissipation; internal friction; bottom or boundary-layer friction; and dissipation into a fluid bottom. Energy losses caused by percolation are negligible on muddy coasts since clays are highly impermeable. Attenuation at the free surface is also negligible, although Hunt and Brampton (1972) have shown that, under certain conditions with a contaminated surface, viscous damping may occur.

In general the energy loss in clear water resulting from internal friction is quite small, as shown by Hough (1896) and Lamb (1932, art. 349). However, when viscosity of water is increased significantly with the addition of sediment particles, to say 1 stoke or more, internal friction may become important, especially for high-frequency waves. Neglecting bottom effects, wave height can be shown to decay exponentially as

$$H = H_o \exp\left(\frac{-32\pi^4 \nu t}{g^2 T^4}\right) \qquad (12)$$

where ν is kinematic viscosity and t is time of travel beginning at t = 0 when wave height is H_o (Keulegan, 1950). Taking wave period = 15 sec, viscosity = 1 stoke, and t = 1000 sec, the time necessary for a solitary wave (H~0.5 m, h~2 m) to travel a distance of 5 km (equation 9), it can be shown that $H = 0.99\ H_o$; essentially no wave energy is lost in this instance to internal friction. Since H varies as the fourth power of wave period, the height attenuation for short-period waves becomes more important. For instance, given a 1-sec wave under the same conditions as above, $H = 0.04\ H_o$, and the wave essentially disappears upon reaching shore after traveling 5 km, the width of a typical mudbank. In a natural situation 1-sec waves will travel somewhat slower than 15-sec waves and therefore, in the hypothetical situation above, may be entirely dissipated before reaching the shoreline. Calculations using equation 12, based on typical wave data gathered from regions of fluid mud, suggest that energy loss is non-negligible over the width of a mudbank for waves up to 3-sec periods. This is important in explaining loss of high-frequency waves with increasing sediment concentration, as shown in Figure 9.

Keulegan (1948) has determined that the theoretical rate of loss of energy owing to viscous shear beneath a solitary wave on a smooth horizontal surface is

$$\frac{dE}{dt} = \frac{4}{\pi^{3/2}} \left(\frac{4}{3}\right)^{1/4} \rho \nu^{1/2} g^{5/4} H^{7/4} \qquad (13)$$

where, again, ν is kinematic viscosity. Since the rate of energy loss must be manifested in the

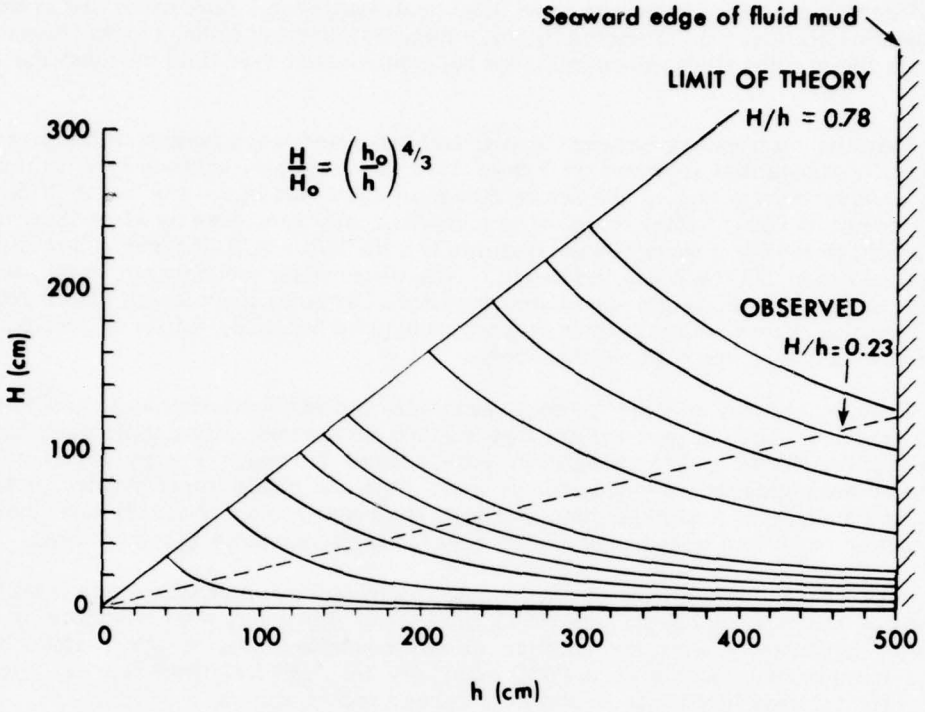

Figure 18. Plot of predicted and observed wave height versus water depth for solitary waves.

amplitude attenuation, the dissipation can be written

$$\frac{dE}{dt} = \frac{dE}{dH}\frac{dH}{dx}\frac{dx}{dt} = \frac{dE}{dH}\frac{dH}{dx}C \qquad (14)$$

where C is given in equation 9. Equations 8 and 14 may be combined to yield

$$\frac{dE}{dt} = -\frac{4}{\sqrt{3}}\rho g^{3/2} h^2 H^{1/2}\frac{dH}{dx} \cdot \qquad (15)$$

Ippen et al. (1955) have shown that equations 13 and 15 may be alternatively written

$$\left(\frac{H}{h}\right)^{-1/4} - \left(\frac{H_o}{h}\right)^{-1/4} = \frac{1}{12}\left[\frac{\nu}{g^{1/2} h^{3/2}}\right]^{1/2}\frac{x}{h} \qquad (16)$$

where H_o is initial wave height and H is wave height after the wave has traveled a distance of x. Laboratory experiments have verified this mathematical form for rate of attenuation (Daily and Stephen, 1953b; Ippen et al., 1955). It is important to note that rate of energy loss resulting from viscous friction is, to a first approximation, the same as that resulting from bottom friction. In each case, rate of energy dissipation per unit area is proportional to the

product of shear stress and horizontal particle velocity at the boundary (Putnam and Johnson, 1949)

$$D_f = \kappa \tau_b u_b \qquad (17)$$

where κ is a friction coefficient. Numerical equivalence can be obtained by selecting appropriate frictional coefficients.

To assess the effect of viscosity on wave attenuation caused by viscous friction, the rate of attenuation (equation 16) was plotted for viscosities of 0.01, 0.05, 0.10, and 1.0 stoke for a constant water depth beginning at an H/h of 0.78 (Fig. 19). Taking a viscosity of, say, 0.05 stoke, a wave in 2 m of water will undergo a relative height attenuation of from 0.78 to 0.45 after traveling 5 km. In a water depth of 2 m this corresponds to a height decrease of from 1.56 to 0.90 m. For viscosity of 1.0 stoke, the corresponding height decrease is from 1.56 to 0.44 m. The range in determined H/h ratios for the two field sites (1 and 2) on Warappabank have been plotted in Figure 19 at the appropriate x/h locations, assuming a mudbank width of 5 km and an average depth of 2 m. These data indicate that kinematic viscosities of 0.1-1.0 in the bottom boundary layer are sufficient to attenuate waves from an H/h = 0.78 to the H/h ratios observed in this study. If initial H/h is less than 0.78, a more realistic condition, then a smaller viscosity is required to achieve the observed rate of dissipation. This effect is clearly significant and may explain in part the steady decrease in wave height.

Although equation 16 was derived for a smooth horizontal bottom, its use is not restricted to laboratory conditions. The nearshore region of the Surinam coast may be considered physically and hydraulically smooth. The fact that bottom slope differs from zero and therefore water depth does not remain constant over mudbanks at a given stage of the tide will normally cause wave shoaling. Thus additional energy must be dissipated by higher near-bottom viscosities in the boundary layer or by other mechanisms.

Gade (1959) has developed a model to explain loss of wave energy resulting from dissipation into a fluid bottom. The motivation for this model was the observation that fluid mud in the "mud hole" of the central Louisiana coast significantly altered wave heights (Morgan et al., 1953; Gade, 1958). Basically, the model required a wave motion within the bottom fluid mud that lagged the surface water wave motion. Tubman and Suhayda (1976) have shown that an oscillating bottom can dissipate energy at a rate at least an order of magnitude greater than that resulting from bottom friction alone. As will be discussed in the next section, it is not known whether fluid mud over mudbanks oscillates vertically while maintaining its cohesive structure; however, clouds of sediment are believed to be suspended with each passing wave, and it is hypothesized that large but unknown amounts of energy are lost in suspending this sediment.

Fluid-Mud Dynamics

Suspension and deposition. The rapid increase in suspended-sediment concentration shown in Figure 13a results from the dispersion of bottom fluid mud into the overlying water column, beginning at or near mid-tide. Data plotted in Figure 14, taken on three different sampling days, show that as water depth decreases as a result of falling tide, suspended-sediment concentration increases exponentially. The coefficient of determination, r^2, indicates that 60 percent of the variation in suspended sediment can be attributed to changes in tide height. The unexplained variability may be due to height of incoming waves. Solitary wave theory predicts that, even for a constant H/h, higher waves have greater bottom velocities. Thus at any given stage of the tide, higher waves may suspend more sediment; as

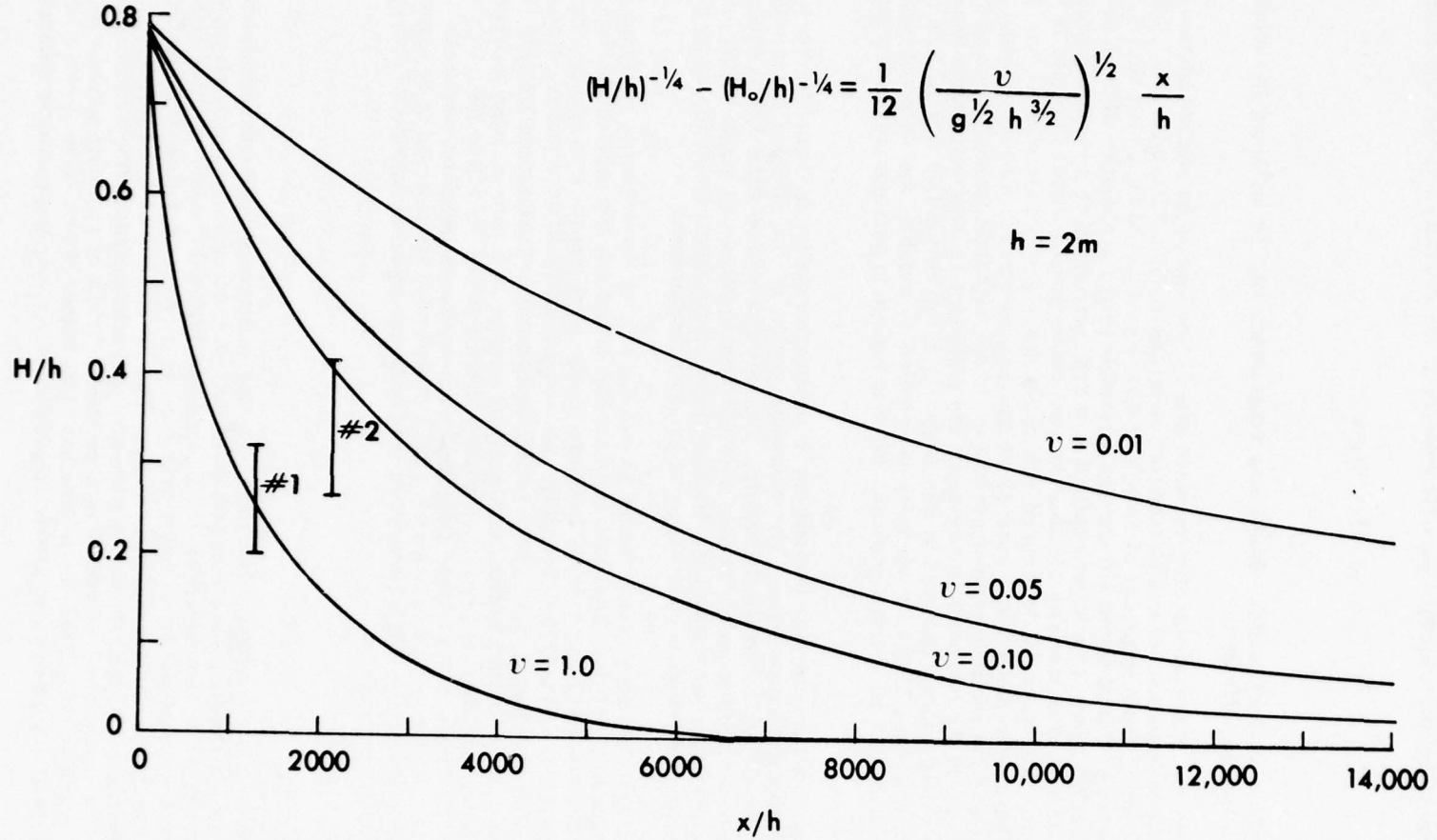

Figure 19. Plot showing effect of viscosity on wave height attenuation due to viscous shear within the bottom boundary layer. The ranges in observed H/h ratios are plotted for field sites 1 and 2 at their appropriate distances (x/h) from the seaward edge of Warappabank.

H increases, so does h, since more fluid mud is suspended, and the ratio H/h remains nearly constant at 0.23. The increase in water turbidity by larger waves has been verified qualitatively from coastal reconnaissance.

As water level rises over mudbanks exposed at LW (Fig. 13b), the surface layers of fluid mud are suspended by waves. The continuous suspension, combined with continuous increase in water level, results in a dilution in concentration. By termination of the experiment shown in Figure 13b, approximately 0.8 m of fluid mud had been suspended and the bottom was effectively lowered by this amount.

In estuaries high suspensate concentrations may also be attributed to the presence of fluid mud such as was found in the Surinam River entrance (Fig. 13c). Each time a mudbank migrates past the river mouth, fluid mud gains entrance to the river and accumulates in the channel as lenses 1-2 m thick. Strong tidal currents sweep mud out during ebb flows, but it returns during flood and concentrations may remain high for several years during the passage of a mudbank. During this process some of the total mud volume is lost to tidal overbank deposition. Examination of water quality data as far back as 1961 in various reaches of the river channel (Hydraulics Research Division, Ministry of Public Works and Traffic, Paramaribo, 1970) reveals that river water contains average suspended-sediment concentrations ranging from 60 mg/l to 22,000 mg/l and that the highest of these values occurred from 1966 to 1968, a time that corresponded with the last passage of a mudbank across the river mouth. Thus as mudbanks migrate westward each river entrance or harbor is periodically inundated with mud that originates as a coastal deposit.

The lack of fluid mud in areas between mudbanks accounts for both the overall low concentrations and the lack of systematic variations in concentration (Fig. 13d). These low values, 15-80 mg/l in surface waters (Table 1), are actually quite typical of concentrations observed on other muddy coasts throughout the world (McCave, 1972). The high concentrations in nearshore water over mudbanks are unusual and, as noted by Wells and Coleman (1977), this water may be the muddiest in the world.

The suspension of fluid mud takes place in two modes, as indicated in Figures 16 and 17: short-term wave-by-wave suspension and longer term suspension related to tide-induced water-level fluctuations. The wave-by-wave density changes in Figure 16 are caused by the suspension of fluid mud with each passing wave. A cloud of sediment, with concentration estimated to be 50,000 mg/l, causes these density changes, as shown diagrammatically in Figure 20. At time t_1, 8 cm of fluid mud covers pressure transducer B. A relatively sharp density gradient extends another 20 cm upward, where density decreases from 1.16 gm/cm^3 to 1.026 gm/cm^3, the density of seawater. At time t_2, the bed is instantly suspended and a dense cloud of muddy water extends to the surface. These sediment clouds were not visible during the experiment because of the ambient high turbidity. This suspension causes the average density between pressure sensors A and B to decrease. The trend toward increasing differential density, beginning at t_3, results from the gradual settling after the wave crest has passed. Velocities given by solitary wave theory (Munk, 1949) indicate that water particles first move at a distance of $x = 10h$ from the crest, but that particle velocities are only 10 percent of maximum values outside the crest region between t_2 and t_3. This may explain the suddenness of the density changes, all of which occur within a 2-3-sec period. Time t_4 represents the return to initial bed state; near-bottom density increases as particles settle during the time between passage of wave crests. Difficulties in explaining this high rate of settling will be discussed later.

The long-term density change at this field site (Fig. 16) is also quite important because it shows that, simultaneous with the suspension of clouds of sediment by waves, a layer of fluid mud is slowly stripped from the bottom near time of low tide. This is the layer of fluid mud that causes the high suspended-sediment concentrations described previously. Between 1245 and 1445 hours (Fig. 16), an estimated 10 cm of fluid mud is removed from the bottom,

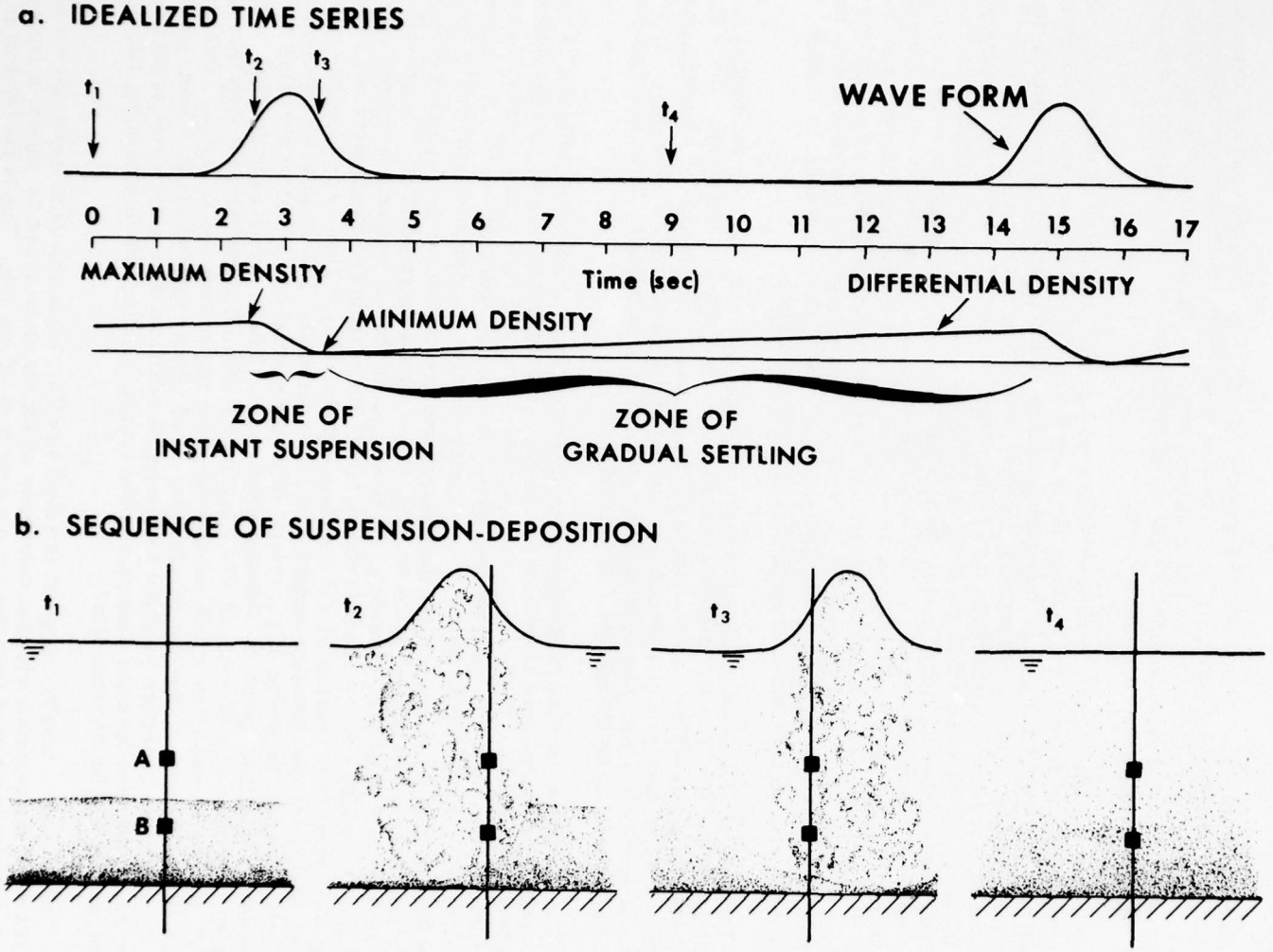

Figure 20a-b. Wave-by-wave near-bottom density changes as explained by sediment suspension and deposition.

much of it during the 10 min from 1245 to 1255 hours. The substantial decrease in wave-by-wave suspension of fluid mud at 1445 hours is caused by the removal of this fluid mud layer over pressure transducer B. Once this fluid mud is removed, pressure transducer B records very nearly the same density changes as pressure transducer A, thus giving a stable differential density record.

Similarly, the dramatic density changes on the intertidal mudbank (Fig. 17) are important in understanding fluid-mud dynamics. Between the hours 1210 and 1335, before water has covered the mudbank, both long- and short-period changes in fluid-mud density occur. These density changes are well within the limits of precision of the pressure-sensing instrument (see Appendix I) and provide evidence that movement of fluid mud takes place while the mudbank is exposed as a tidal flat. The propagation of solitary-like waves through fluid mud and the transport of clay particles in clear water overlying the fluid mud are other indicators that intertidal banks of fluid mud are not stagnant deposits.

Another important feature of Figure 17 is the sharp change in slope between time series sections D and E, at a time when surface waves were 10 cm high. Ariathurai and Krone (1975) reported that at bed shear stresses just above the critical value in cohesive sediments erosion takes place particle by particle, whereas at higher stress levels the bulk shear strength of the bed is exceeded and it fails totally, resulting in instant suspension. The rapid density decrease in section E may correspond to such a mass erosion phase that leads to rapid and complete dispersion of fluid mud into water. Unfortunately, no data are available after mid-tide and further details of this process cannot be determined. It is known, however, that fluid mud is redeposited at high tide, a conclusion originally based on the clear appearance of the surface water and later verified by near-bottom sampling and fathometer profiling.

Controversy presently exists over whether fluid mud can be transported as a mass by a creeping motion from shear exerted by overlying water. NEDECO (1965) and Ippen (1966) report that such mass movement occurs in nature, although it has never been measured directly. Parthenaides (1971) and Krone (1962; 1972) feel that this is not possible and that mud must first be suspended. Evidence from visual observation, such as bottleneck failures, indicates that mass movement without suspension takes place in the special case when fluid mud is exposed as a LW tidal flat.

The related question of whether or not the fluid-mud bottom oscillates vertically while maintaining its cohesive structure cannot be answered from this study. Documentation of "mud wave" movements in soft Mississippi Delta muds (Suhayda et al., 1976; Tubman and Suhayda, 1976) suggests that this is likely to occur in Surinam; however, a "mud wave" amplitude of 15 cm would be required to explain the wave-by-wave density changes observed in this study. A reasonable assumption is that some vertical movement takes place near the base of the fluid mud, but that the density changes can be caused only by large amounts of mud moving as a suspended sediment above pressure transducer A (Fig. 20).

Velocities necessary to initiate suspension of cohesive sediment have generally been determined in the laboratory. Considerable discrepancy exists in the literature. For example, Zenkovitch (1967) reported that fine silts are "stirred" at near-bottom velocities of 7-12 cm/sec, whereas NEDECO (1968) reported that fluid mud is not suspended until velocities of 70 cm/sec are achieved. Other studies show that, in a single series of experiments, a considerable range is possible: Allersma et al. (1967), 20-100 cm/sec for Chao Phya muds; and Delft Hydraulics Laboratory (1962), 10-90 cm/sec for British Guiana muds. For cohesive sediments in general, Drake (1976) suggested that average velocities of 10-30 cm/sec at 100 cm above the bed are necessary to initiate erosion. Use of early diagrams from Hjulstrom (1935) and Sundborg (1956), as reported by Parthenaides (1971), indicate values of 18 cm/sec for erosion of unconsolidated cohesive sediments. Although no current data were taken over banks of fluid mud, estimates of wave-induced currents, taken from solitary wave theory, reveal the large magnitude of bottom currents even for small waves

(Fig. 21). On the basis of our present state of knowledge, these wave-induced currents from 50 to 100 cm/sec are sufficient to suspend fluid mud.

The rapid settling, then re-formation, of a fluid-mud layer during a wave period is contradictory to one's intuitive expectation. Generally fluid mud forms slowly in quiet areas such as settling and turning basins or, during certain stages of the tide, in river channels. For individual particles, provided that concentrations are low, settling rate is given by the equation for Stokes settling velocity

$$V_s = \frac{1}{18} \frac{\rho_s - \rho}{\mu} g D^2 \qquad (18)$$

where μ is dynamic viscosity. Median particle size of dispersed clays in Surinam is approximately 1 micron or less (Fig. 15). In clear, saline water, a 1-micron clay particle will settle at 1×10^{-4} cm/sec or about 1 m in 12 days. Clearly this settling rate is many orders of magnitude too low to account for the rapid deposition observed in this study.

In water where salinity exceeds 1 °/∞ , clay-sized particles aggregate into flocs due to electrostatic or organic bonding (Whitehouse and Jeffrey, 1954; Krone, 1962, 1972). Examination of Surinam muds verified the existence of such flocs; Delft Hydraulics Laboratory (1962) reported that flocs in nearby British Guiana muds had diameters of 7-12 microns. The settling velocities of aggregates rather than individual particles are often used to explain the rapid deposition rates in muddy regions. Krone (1972) found that flocs in Savannah Harbor having Stokes settling diameters of $4\text{-}10 \times 10^2$ microns settled from 0.45 to 3.30 cm/sec. According to Krone, a 6×10^2 micron aggregate contains about half a million particles.

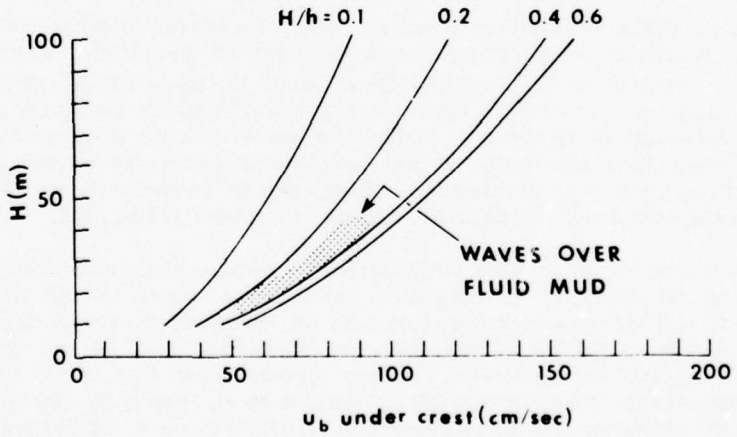

Figure 21. Theoretical bottom particle velocities under solitary wave crests.

Settling velocities equal to those observed by Krone (1972) in Savannah Harbor are sufficient to explain the deposition that takes place after sediment is suspended by the tide. However, these rates are still insufficient to explain deposition during a wave period. An average settling rate of 5-10 cm/sec is needed for the rapid mud deposition after the passage of a wave crest, as proposed in Figure 20. This is the settling rate of quartz spheres 1-2 mm in diameter. Quartz sands on many U.S. East Coast beaches are smaller than this, and it is difficult to visualize mud flocs of this equivalent hydraulic diameter.

The accepted mode of settling at concentrations greater than approximately 10,000 mg/l is one of "hindered settling" whereby interparticle contact is maintained and water is expelled slowly as the mass settles (Krone, 1962). In contrast to this finding in the literature, results of this study indicate that particles may settle as a unit, a mass that fails under the shear of a passing wave but rapidly regains its structure as a fluid mud during the settling process, then forms an interface that quickly collapses to give an overall high settling rate. The formation of such mud-water interfaces during settling has been observed by several scientists, most notably Pierce and Williams (1966) and Owen (1970). Although laboratory settling rates for interfaces are ordinarily no more rapid than for "hindered settling," field data from several studies suggest that settling may actually be faster under natural conditions and that low-energy environments are not a prerequisite for rapid settling. For example, Owen (1969) found that on Thames muds in situ settling velocities were an order of magnitude higher than for those determined under quiescent laboratory conditions, and McCave (1971) found that in the North Sea suspended-sediment deposition could take place regardless of the value of a "wave effectiveness parameter" for sediment scour.

Mud transport. The important finding in this study that the wave profile over banks of fluid mud is very close to that given by solitary wave theory has been utilized to assess the role of waves in transporting sediment. Wave height and water depth, together with computed wave length (equation 1) for each wave record in Figure 10, show that waves over mudbanks are clearly within the application bounds for solitary wave theory, as presented diagrammatically by Komar (1976; Fig. 22). Although only wave form and wave period have been measured in the field, according to Munk (1949) a solitary-like profile alone suggests application of this theory. This is perhaps true because, unlike most wave theories, solitary wave theory was developed to describe what had been observed previously in nature. Extensive laboratory studies by Daily and Stephen (1953a) and Ippen and Kulin (1955) have shown that if wave form is given by equation 2, then the overall behavior of the waves is described by solitary wave theory.

Assuming that waves over mudbanks can best be described by solitary wave theory, then the potential for longshore sediment transport is high for three reasons. First, horizontal and vertical water particle velocities under a solitary wave, given, respectively, by

$$u = CN \frac{1+\cos(My/h)\cosh(Mx/h)}{[\cos(My/h)+\cosh(Mx/h)]^2} \qquad (19)$$

$$w = CN \frac{\sin(My/h)\sinh(Mx/h)}{[\cos(My/h)+\cosh(Mx/h)]^2} \qquad (20)$$

show that there is no reversing or oscillatory flow, so that water moves only in the direction of wave travel. Second, deepwater wave statistics compiled by NEDECO (1968) from 40 years of observations indicate that 93 percent of sea and swell waves approach the coast between N30°E and east; because of this direction of wave travel, there is a strong year-around longshore component. Third, as given in Table 1, suspended-sediment concentration is

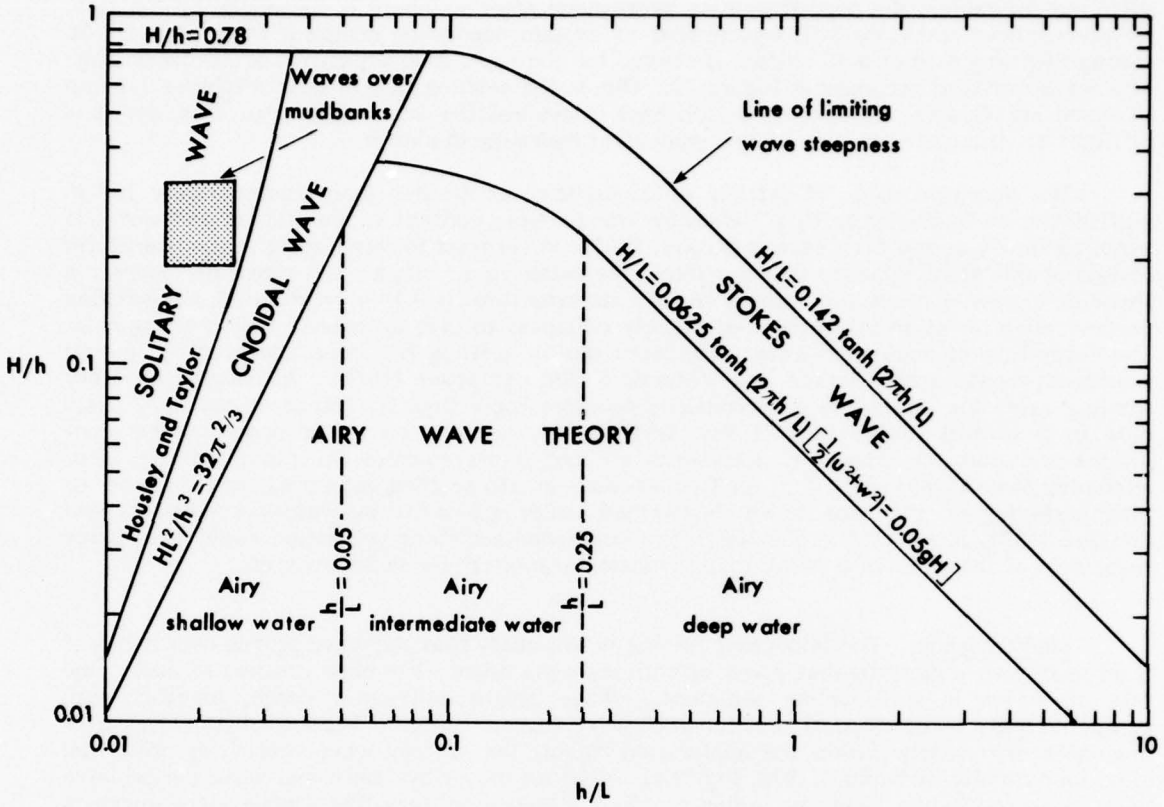

Figure 22. Generalized wave validity diagram showing regions of applicability of several wave theories (from Komar, 1976). Note region of waves over mudbanks in Surinam.

high in water over mudbanks where solitary-like waves are present. Temporarily ignoring other coastal processes, the net outcome will be a sediment-laden water that moves only shoreward with a strong westward component.

In previous investigations along the Surinam coast waves were considered mainly as an important eroding and suspending agent (NEDECO, 1968). Sediment transport over long distances, such as between the Amazon and Orinoco Rivers, was attributed to the swiftly flowing Guiana current. Estimates of sediment transport along the northeastern coast of South America are given variously in tons and cubic meters and by month and season. These estimates, taken from Delft Hydraulics Laboratory (1962), Gibbs (1967), Allersma (1968), NEDECO (1968), and Eisma and van der Marcel (1971), can be summarized as follows. Approximately 20-40 percent of the total load from the Amazon River is transported northwest along the coast. This amounts to 150 x 10^6 m^3/yr of "through transport" in the form of suspended sediment and another 100 x 10^6 m^3/yr that moves in the form of mudbank propagation. Thus a total of 250 x 10^6 m^3/yr moves in a band that extends from the shoreline

to 30 km offshore. These estimates were based on volume and rate of mudbank migration, average residual current speed, and suspended-sediment concentration on the continental shelf. In the following paragraphs, volume transport that can be explained by currents associated with solitary waves is examined.

Consider mass transport to be given by

$$T_M = cAv \tag{21}$$

where c and v are time and depth averages. If bulk density of the transported mass after deposition is known or assumed, then volume transport is found by dividing by sediment concentration at that density

$$T_v = \frac{T_M}{\rho_c} \quad . \tag{22}$$

Next, consider transport to be through a cross-sectional area determined from the width of the mudbank and average water depth (Fig. 23). Since the longshore component of transport depends on angle of wave approach, equation 22 becomes

$$T_v = \frac{cAv \sin \alpha}{\rho_c} \quad . \tag{23}$$

Again assuming that solitary wave theory provides a reasonable description of waves over mudbanks, the total volume per unit crest length above SWL can be obtained as

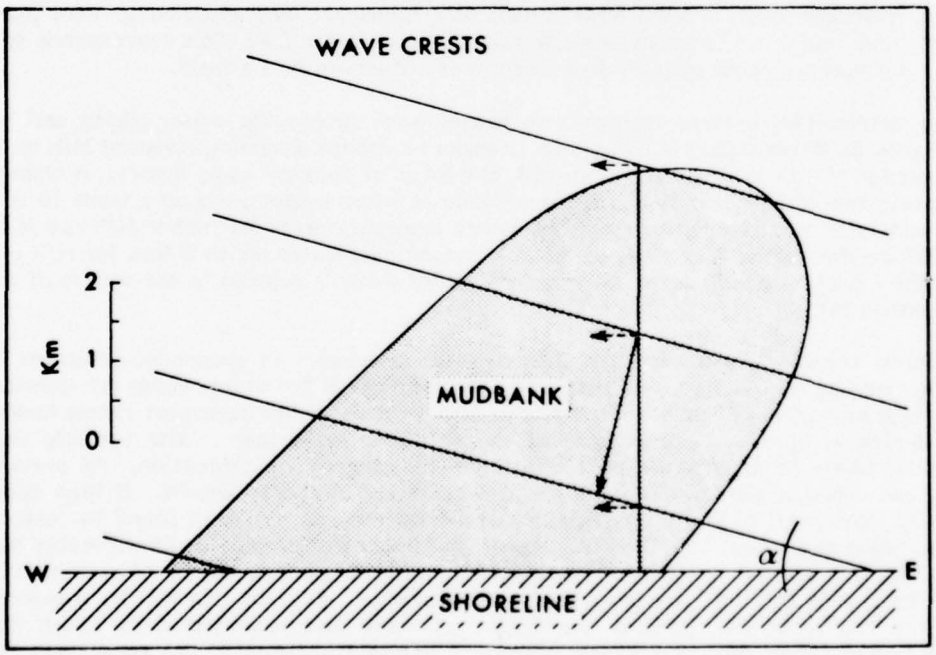

Figure 23. Idealized mudbank, coast of Surinam. Dashed lines represent longshore components of wave drift.

$$Q = \int_{-\infty}^{\infty} \eta dx = 2 \int_{0}^{\infty} \eta \, dx \qquad (24)$$

where the substitution of equation 2 for η yields

$$Q = 2 \int_{0}^{\infty} H \operatorname{sech}^2 \left[\sqrt{\frac{3}{4} \frac{H}{h^3}} (x - Ct) \right] . \qquad (25)$$

Munk (1949) integrated equation 25 to obtain, to a good approximation,

$$Q = 4h^2 \sqrt{\frac{1}{3} \frac{H}{h}} . \qquad (26)$$

Since a volume transport equal to Q takes place during one wave period, T, the mean transport per unit time equals Q/T and volume transport velocity, averaged from the surface to the bottom, yields

$$\bar{V} = \frac{Q}{hT} = \frac{4h(1/3\ H/h)^{1/2}}{T} . \qquad (27)$$

Equation 27 has units of LT^{-1} since Q is taken to be volume per unit length of wave crest. Substitution of equation 27 into equation 23 for velocity allows a more rapid determination of sediment transport since particle velocities under a solitary wave must be integrated numerically for each wave of different H/h ratio. Comparable results are obtained using either particle velocities or average volume transport rate of water.

Table 3 gives values of longshore transport per year for solitary waves of 15-sec period arriving at the shoreline at a 10° angle. Suspended-sediment concentration was taken to be 2000 mg/l, averaged over a 5-km-wide mudbank. Transport was assumed to take place 3 hours each tidal cycle, 1.5 hours before LW and 1.5 hours after LW. This corresponds to the length of time that the most solitary-like waves were observed in the field.

The determined volume transport increases with increasing water depth and wave height. Figure 24 shows this rate of volume transport increase assuming constant H/h of 0.23, that observed in the field (Fig. 10), and 0.78, the limit of solitary wave theory. A change of approximately two orders of magnitude takes place as wave height increases from 10 to 100 cm, maintaining a constant H/h ratio. The lower transport rates for higher H/h ratios (0.78 versus 0.23) are due to the fact that, for given wave height, water depth is less for H/h = 0.78 than for H/h = 0.23, and volume of water in a solitary wave is related to the square of water depth (equation 26).

Volume transport will increase linearly with increases in suspended-sediment concentration, cross-sectional area, and portion of the tidal cycle for which waves are considered solitary. Higher angles of wave approach will also lead to higher transport rates; however, only low angles of approach are present at the shoreline in Surinam. The variable that is perhaps most likely to affect transport is suspended-sediment concentration. As previously discussed, the vertical distribution of suspended sediment is poorly known. If high concentrations, say 2000 mg/l to 20,000 mg/l, travel near bottom, as has been found for estuarine fluid muds (Inglis and Allen, 1957), then the average concentration may be considerably higher than the 2000 mg/l taken here. As discussed in the last section, clouds of sediment with concentrations of 50,000 mg/l are suspended by each wave. Much of this will be transported. Further, the transport calculations are based on wave and sediment data taken during September and October, the two calmest months of the year in terms of sea conditions. Data taken during rough-season months may increase these values significantly.

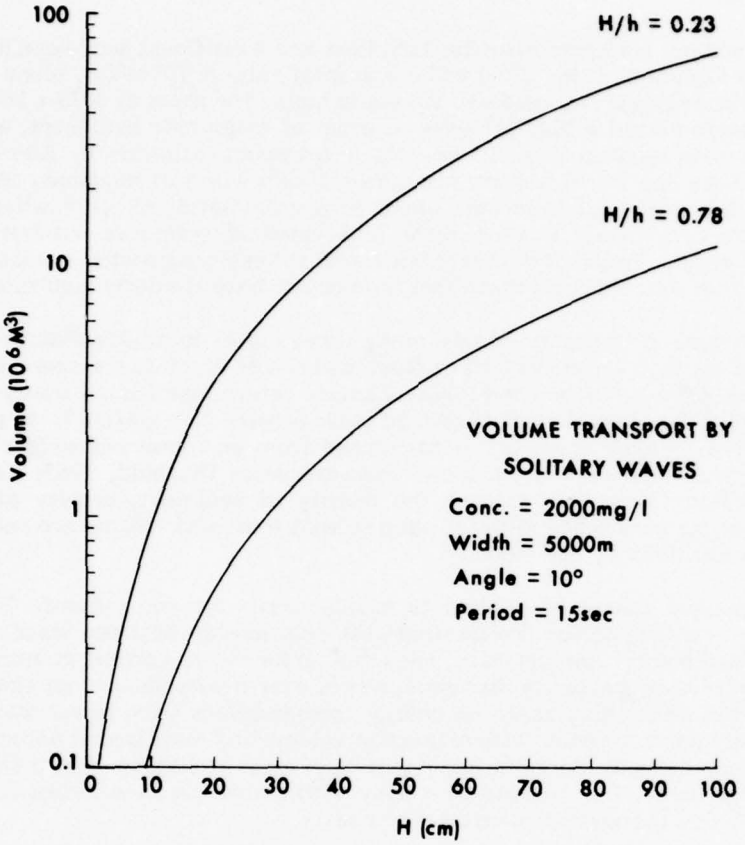

Figure 24. Volume transport of sediment by solitary waves for H/h = 0.23 (observed) and H/h = 0.78 (theory).

Table 3

Longshore Volume Transport of Mud ($10^6 m^3/yr$) by Solitary Waves As a Function of Wave Height and Water Depth

	H (cm)				
h(cm)	30	40	50	60	70
70	2.70	3.12	3.48	*	*
90	3.92	4.52	5.10	5.58	6.02
110	5.30	6.12	6.84	7.56	8.16
130	6.84	7.58	8.78	9.66	10.46

*H/h exceeds 0.78.

NOTE: Values were determined for T = 15 sec, $\alpha = 10°$, c = 2000 mg/l, W = 5 km.

Typical volume transport rates for U.S. East and West Coast sand beaches range from 1 to 3 x 10^5 m^3/yr (Johnson, 1956; 1957) and a transport rate of 10^6 m^3/yr, found on some high-energy California beaches, is considered unusually high. The rates of 3-70 x 10^6 m^3 calculated above for mudbanks (Table 3; Fig. 24), even as order of magnitude estimates, are perhaps 100 times higher than on sandy coasts. If the volume transport estimates by Allersma (1968) and NEDECO (1968) are applied to a 5-km instead of 30-km width of mudbank, then the volume transport over this region of fluid mud would be approximately 42 x 10^6 m^3/yr. Thus wave-induced currents can readily explain these high rates of transport without the aid of a superimposed current. Zenkovitch (1967) has found volume transport in the Gulf of Po Hai to be 10^6 m^3/yr, a fact that suggests that other mud coasts have similarly high rates.

Although volume transport may be many times higher in muddy than in sandy environments, owing to the high water content of fluid mud (Table 2), mass transport may actually be less. The values given in Table 3 and Figure 24 were determined from a transported sediment concentration of 250 kg/m^3, that of fluid mud (bulk density 1.18 gm/cm^3). In studies on sand and coral beaches, volume transport is calculated from an immersed weight transport rate that is determined empirically from wave characteristics (Bagnold, 1963; Komar, 1976, p. 206). This method takes into account the density of sediment, density of water, and a correction factor for pore space in beach sand so that mass and volume are related, as in the present study, essentially by bulk density.

This technique cannot be applied to muddy coasts for two reasons. First, sufficient field data are not available for "calibrating" the relationship between wave characteristics and immersed sediment transport rate when the sediment is carried in suspension as clay aggregates. Second, as previously discussed, waves over mudbanks are not sinusoidal and the application of this technique, based on energy considerations from linear wave theory, may not be valid. An important point with respect to volume and mass is that volume transport on muddy coasts may actually be more important than mass transport. Since fluid mud occurs regularly as large banks that migrate as a body with delineable boundaries, it is volume and not mass of the body that affects coastal processes.

Several simplifications that require qualitative evaluation have been introduced into the transport calculations. The longshore component of net drift has been determined under the condition that no coastal boundary exists. This is clearly unreasonable. The shoreward-directed net drift component requires a compensating return flow to satisfy continuity considerations. However, if a uniform return flow is taken perpendicular to the coastline, which is common procedure for solitary wave applications (Munk, 1949), then longshore transport is unaffected. An alternate method for return flow is through the generation of rip currents. There is some field and laboratory evidence, cited by Munk, that in the case of solitary waves a slight but continuous seaward movement of bottom water does take place, thus suggesting that rip currents alone do not fully balance the shoreward transport of water.

Longshore circulation patterns, in which rip currents may be a part, have also been ignored. Because of the irregular nearshore topography resulting from the presence of mudbanks, waves are refracted, giving rise to localized convergence and divergence of wave energy. According to Allersma (1968) and NEDECO (1968), convergence of wave energy is in the area between mudbanks, whereas divergence is over mudbanks. Based on this, each concludes that shoreward transport of water is between mudbanks and seaward transport of water is over mudbanks.

Some doubt may be attached to these conclusions. The normal wave refraction pattern is for wave convergence over offshore shoals and shoreface-attached ridges (Goldsmith, 1976), even if their trend is oblique to the shoreline such as along the Surinam coast. The refraction diagrams presented by Allersma (1968) and NEDECO (1968) are considerably oversimplified and are constructed for an idealized mudbank; different results can be obtained by selecting different wave ray spacings and angles of approach.

The importance of the areas of convergence is that they give rise to higher waves. Longshore currents are then generated from the longshore gradient in wave energy. This, in turn, may set up a circulation cell so that return flow takes place in areas of wave divergence. Even though waves are higher between mudbanks, where they expend their energy as plunging breakers, it is possible that a greater wave set-up occurs over the mudbanks, owing simply to the translatory nature of solitary-like waves. If this is the case, then an onshore-offshore flow pattern opposite to that proposed by Allersma (1968) and NEDECO (1968) would follow. Recent work by Sonu (1972) on the west coast of Florida documents a shoreward current over shoals, where waves break by spilling, and a return flow in troughs, where waves break by plunging.

In connection with nearshore circulation, currents measured 5 km offshore at field site 4 indicate that a substantial residual current is present. Closer inshore, the effects of the Guiana current are unknown but are believed to be considerably less, especially over mudbanks. As pointed out by Komar (1976, p. 203), the belief that tidal currents and ocean currents approach close to shore and were primarily responsible for longshore transport has been replaced by the concept of wave-induced longshore currents as being the chief cause of sediment movement.

Data from NEDECO (1968) indicates that at a distance of 20 km offshore, residual surface currents range from approximately 20 to 40 cm/sec, depending on longitude and season. This is a distance offshore where sediment concentrations are low. In this study it is believed that most of the sediment transport takes place where thick accumulations of fluid mud are present. The complete suspension of fluid mud to a distance offshore of perhaps 5 km, then transport by waves, may carry far more sediment than the continuous residual current in low-concentration areas.

Studies by Eisma (1967) and Gibbs (1975) have shown that mud derived from the Amazon River is trapped in the nearshore region by net shoreward-flowing bottom currents. Once in this coastal region, the major transport may be due to wave-associated currents and circulation. The wave/fluid-mud interaction tends to be self-perpetuating; once waves become solitary-like, they transport the sediment both shoreward and alongshore, so that mudbanks may move by the transport of fluid mud.

Implications to Other Coasts

"Mudflats" and "mangrove flats" represent 23 percent of the total coastline in North and South America (Dolan et al., 1972) and perhaps a similar percentage worldwide. At least five muddy coasts that are open and thus exposed to incoming waves have accumulations of fluid mud: central Louisiana coast (Morgan et al., 1953); northeastern coast of South America (Delft Hydraulics Laboratory, 1962; NEDECO, 1968); Gulf of Thailand (NEDECO, 1965); Gulf of Po Hai (Zenkovitch, 1967); and southwestern coast of India (Moni, 1970; Nair, 1976). In addition, many estuaries such as San Francisco Bay (Krone, 1962) and Delaware Bay (Simmons, 1966) and river entrances such as the Mississippi (Bates, 1953; Fisk et al., 1954; McClelland, 1967) and Severn (Kirby and Parker, 1973) are partially filled with tenacious fluid mud. The new information gained in this study may be important to understanding suspension, deposition, and transport dynamics in these and other coastal regions.

On each of the muddy coasts above where fluid mud is present, two features are common: high suspended-sediment concentration and extraordinary change in wave form. A major implication of this study, then, is that if waves moving over a fluid-mud boundary have characteristics of solitary waves, then sediment transport by waves alone is possible. In fact, inasmuch as solitary-like waves have been observed where suspensate concentrations are highest, namely over fluid-mud deposits, then in each of these areas transport of sediment by waves may exceed transport by stronger offshore currents where sediment concentrations are

lower. Thus an appropriate explanation for sediment transport in muddy-coast environments may require a combination of wave-associated currents in the nearshore fluid-mud region and a residual oceanic current farther offshore. Furthermore, high volume transport rates, say greater than 10×10^6 m^3, are possible without breaking waves and utilization of the concepts of radiation stress and a nearshore circulation cell, as normally applied to sandy coasts (Komar, 1976, p. 170), even though such patterns of circulation may occur.

Before the importance of mud transport by waves can be further evaluated, detailed field measurements must be undertaken. At present less than 10 percent of the continental shelf areas have been studied for suspended sediment (Drake, 1976) and detailed wave and current data are available for an even smaller percentage.

CONCLUSIONS

Analysis of field data has shown that shallow-water waves, fluid mud, and suspended sediment interact in the nearshore region of the Surinam mud coast. These interactions are not always straightforward and may be contradictory to findings in sandy-coast environments.

The presence of a fluid-mud bottom affects incoming waves by changing their form from sinusoidal to solitary-like and by preventing wave breaking except for occasional spilling. Measurements from two field sites indicate that as solitary-like waves 12-16 sec in period and 10-50 cm high propagate shoreward, their wave height to water depth ratio, H/h, remains nearly constant at 0.23, regardless of water depth. At higher suspended-sediment concentrations, troughs become flatter and the solitary-like appearance becomes more pronounced. When examined by Fast Fourier techniques, periodic solitary-like waves with flat troughs and a sech^2 crest profile give rise to a distribution of wave energy that characteristically contains harmonics.

It is concluded that the absence of high-frequency waves ($T < 3$ sec) in solitary wave troughs may be due to internal friction from the increased viscosity of water by the addition of sediment particles. The steady decrease in wave height without breaking, up to the shoreline, is explained in part by energy dissipation within the bottom boundary layer. Substantial but unknown amounts of wave energy may be lost by bottom oscillations and sediment suspension. An important conclusion concerning wave attenuation is that muddy coasts tend to protect their shorelines, particularly the fluid mud portions, since wave energy is often dissipated entirely before waves reach the shoreline.

As solitary-like waves move across a mud bottom, the soft fluid mud is suspended rapidly. On a wave-by-wave basis, near-bottom measurements indicate that fluid-mud density undergoes changes of up to 0.05 gm/cm^3 during a wave period, approximately 4.5 percent of overall near-bottom density; to produce these periodic density changes requires the suspension and deposition of a sediment cloud with a concentration of 50,000 mg/l. Inasmuch as present theories and observations cannot explain fully the rapid settling of such a sediment cloud, it is suggested that a collapsing interface is formed where interparticle contact is maintained. Additional studies must be undertaken to determine the extent of vertical oscillations similar to those found in Mississippi Delta muds.

It appears that mudbanks undergo substantial change in time and space from the longer term suspension and redeposition of up to 0.8 m of fluid mud that is related to stage of the tide. The overall high suspended-sediment concentrations at LW, approximately 4000 mg/l in coastal surface waters, are explained by this suspension. The exchange between fluid mud and suspended sediment may cause a near-bottom fluid mud density decrease of from 1.16 to 1.05 gm/cm^3 in a 3-hour period of time.

The presence of solitary waves, high suspended-sediment concentrations, and a relatively uniform angle of wave approach throughout the year may lead to extraordinarily high sediment transport rates. If waves are assumed to have a net drift given by solitary wave theory, then in taking angle of wave approach and actual measured concentration of sediment in suspension, enough sediment can be transported by waves alone to explain the propagation of mudbanks by fluid-mud transport. Based on reasonable wave and sediment conditions, 3-70 x 10^6 m^3 of mud can be transported alongshore each year. An important point concerning high-volume transport rates found by taking this approach is that they do not require breaking waves and the concept of radiation stress and a nearshore circulation cell, as normally applied to sandy coasts.

Although data were collected on one mudbank only, on the basis of extensive aerial reconnaissance it is concluded that solitary waves, high suspended-sediment concentrations, and similar wave-mud interactions occur along other parts of the Surinam coast where fluid mud is present and occur perhaps as far northwest as the Orinoco River and as far southeast as the Amazon River. A closer examination of wave-mud interactions offers possibilities for substantially increasing and quantifying our knowledge of sediment transport in the nearshore. Application of these results to other muddy coasts where fluid mud is present and suspended-sediment concentrations are high is considered appropriate.

APPENDIX I

Wave/Fluid-Mud Pressure Gage

Fundamental to an understanding of fluid-mud dynamics is knowledge of the details of suspension of fluid mud by waves. Unsteadiness of the sediment-suspending fluid precludes the use of sampling devices that are designed for uniform, steady flows. Therefore, a continuously recording prototype instrument, referred to here as a wave/fluid-mud pressure-sensing device, was designed and constructed by the technical staff at Coastal Studies Institute. This instrument has the important feature of being capable of monitoring remotely both mean and fluctuating components of near-bottom or subbottom density changes and at the same time obtaining a time history of surface-water waves or tidal elevation changes. Although pressure transducers have been used in a variety of oceanographic instruments for many years, such a system as this could not be obtained commercially.

The system contains three basic components: two Statham model PA-506 Amplibridge pressure transducers; an electronic readout package; and a two-channel Gould Brush strip-chart recorder (Fig. I.1a). Each pressure transducer has a pressure range of 8.9632×10^5 to 2.2753×10^6 dynes/cm^2 (13-33 psia), which is amplified to give a 0- to 5-volt nominal output over this range. A 100-m conductor cable connects each transducer to the electronic readout, where pressure fluctuations appear on a panel meter. If desired, the signal can be recorded continuously on strip-chart recorder. Three option switches are available on the readout: a filter selector for real-time or filtered output; a mode selector that gives the option of recording waves only, waves and differential density, or water elevation and differential density; and a multiplier selector to increase resolution when taking filtered data with small density changes. The readout and strip-chart recorder are battery powered. Chart speed range is from 1 mm/sec to 50 mm/sec.

The concept of pressure variation in a moving fluid is the basis for this system. Pressure under a wave, less atmospheric pressure, is given by

$$P = \rho g \frac{\cosh\,[2\pi(z+h)/L]}{\cosh\,(2\pi h/L)} \frac{H}{2} \cos\left(\frac{2\pi x}{L} - \frac{2\pi t}{T}\right) - \rho g z \,. \qquad (I.1)$$

The first term in this equation is a dynamic component resulting from kinetic energy of water motion; the second term is a static component resulting from water level changes associated with the wave form. Since in the linearized case $\eta = H/2 \cos(2\pi x/L - 2\pi t/T)$, equation I.1 can be written

$$P = \rho g \eta \frac{\cosh\,[2\pi\,(z+h)/L]}{\cosh\,(2\pi h/L)} - \rho g z \,. \qquad (I.2)$$

This can now be expressed as

$$P = \rho g\ (\eta K_z - z) \qquad (I.3)$$

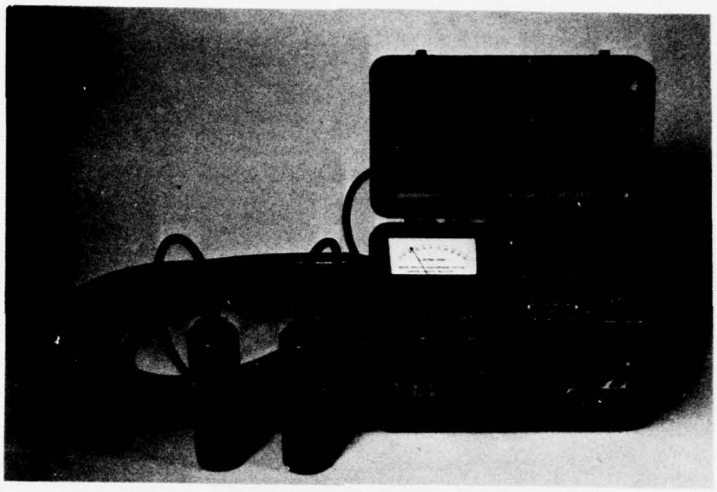

Figure I.1a. Wave/fluid-mud pressure-sensing device (recorder not shown).

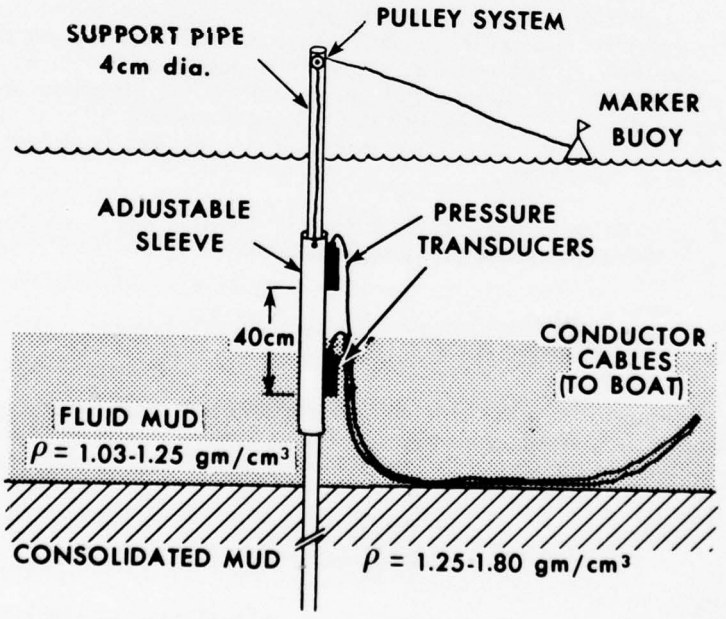

Figure I.1b. Schematic of field setup for wave/fluid-mud pressure-sensing system (see Fig. 2).

where $K_z = [\cosh [2\pi(z+h)/L]]/(\cosh (2\pi h/L))$ is the pressure response factor. In shallow water $h/L < 0.05$, $K_z \rightarrow 1$, and equation I.3 reduces to

$$P = \rho g (\eta - z) = \rho g H_z . \qquad (I.4)$$

This is identically the hydrostatic pressure equation so that, when dealing with solitary waves, pressure to a first approximation is that of the static component only. Values of K_z at the bottom as a function of water depth and wave length are tabulated in CERC (1973) and show that wave attenuation with depth in shallow-water situations is negligible. Thus the difference in hydrostatic pressure at two depths below the surface, H_A and H_B, where $P_A = \rho g P_A$ and $P_B = \rho g H_B$, can be written as

$$P_B - P_A = \rho g (H_B - H_A) . \qquad (I.5)$$

If $H_B - H_A$ is constant with time, then any change in $P_B - P_A$ is directly proportional to a density change.

Applying the above hydrostatic pressure concept in the field, two pressure transducers, A and B, are mounted securely to a vertical pipe with a known distance between them, $H_B - H_A$ (Fig. I.1b). An adjustable sleeve arrangement allows the depth of measurement to be varied so that, if desired, both transducers can be raised out of the fluid mud to record wave data only. Hydrostatic pressure resulting from water (or fluid mud) head is nulled out of each pressure transducer by a potentiometer located on the instrument panel. At the beginning of each experiment, differential pressure, $P_B - P_A$, is zero; only a change in density between the pressure transducers will cause the output to deviate from zero.

Figure 2 shows the two arrangements of pressure transducers relative to the fluid-mud surface. The first arrangement is used to monitor surface waves on one channel and simultaneous density changes at the fluid-mud/water interface on the other channel. This was the normal method of operation at site 1. The second arrangement is used to record long-term density changes in fluid mud resulting from tidal elevation changes. In this case both transducers are placed in the fluid mud, as shown at site 2. As long as surface waves are absent on the fluid-mud surface, the upper transducer will record SWL elevation changes. When used in either fashion, channel 1 is recorded in real-time (equation I.4) and channel 2 is recorded as the difference between filtered A and filtered B (equation I.5). Best results were obtained on channel 2 by using a filter with 20-sec time constant and a resolution increase of 10x.

Prior to the field experiments in Surinam, each pressure transducer was calibrated electronically in the laboratory so that an input voltage equivalent to a force of 10.05215×10^4 dynes/cm^2 (1.458 psi) was recorded as a 1-m hydraulic head. This is the force exerted by a cubic meter of clear seawater with Te = 15°C, S = 33.70 ‰, and weight density = 1.025 gm/cm^3 (64.0 lb/ft^3). These may be considered "average" seawater conditions; adjustments in calibration can be made for specific localities.

The introduction of high concentrations of sediment into seawater will increase density. To evaluate the effect of suspended sediment on wave height as determined by pressure-sensing devices (equation I.4), Table I.1 was prepared for concentrations of a range normally observed in Surinam. Seawater density was calculated using Te = 30°C, S = 34.75 °/$_{oo}$, and specific gravity of sediment particles = 2.65. At concentrations less than 50,000 mg/l, the effect on density is small enough that the difference between apparent and actual wave height can be neglected. Concentrations greater than 100,000 mg/l may significantly affect recorded wave height; however, at no time during the field study did the average concentration of the

entire water column change by 100,000 mg/l with the passage of waves.

The wave/fluid-mud pressure gage was field calibrated by taking samples of fluid mud between the sensing diaphrams of pressure transducers A and B and returning them to the laboratory for bulk density determinations (Appendix III). By doing this, initial bulk density can be established when $P_B - P_A = 0$. Any long-term deviations from the zero pen position are recorded as equivalent water height changes and can readily be converted to density changes using calibration information and equation I.5.

Complications arise, however, when trying to determine density change from equivalent water height change on a short-term wave-by-wave basis. The RC response curve for a filter with a 20-sec time constant (Fig. I.2a) shows that output amplitude for waves of period less than five time constants (100 sec) is less than 100 percent of input amplitude. Thus the signal from the higher frequency waves tends to be attenuated. Further, output amplitude depends on wave shape, so that in natural situations, where the shape of each wave may differ from the preceding wave, an exact differential density scale cannot be determined. For waves over mudbanks in Surinam, the scale for near-bottom density changes resulting from passing gravity waves was simplified by taking an idealized cosine wave 2 sec in duration and 15 sec in crest-to-crest period (Fig. I.2b).

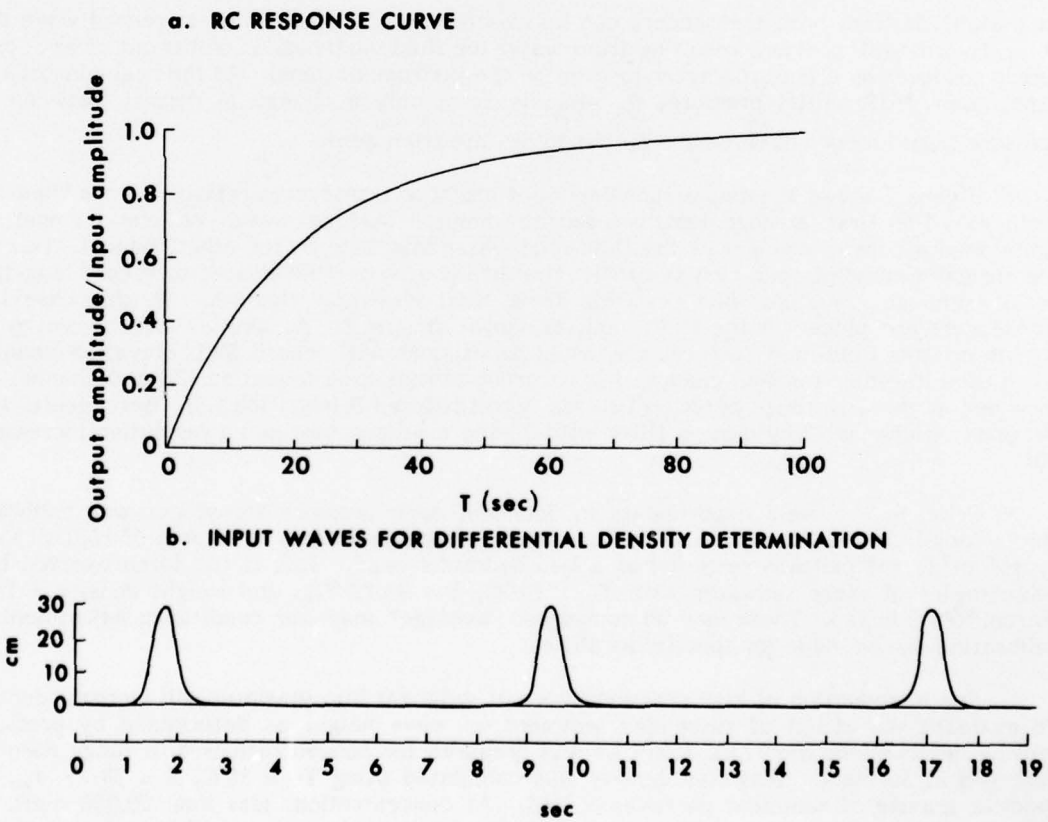

Figure I.2a-b. RC response curve for 20-sec time-constant filter (I.2a); input waves used for output amplitude/input amplitude ratio determination (I.2b).

Table I.1

Effect of Suspended Sediment on Recorded Wave Height
As Determined by Pressure-Sensing Instruments

Sediment Concentration (10 mg/l)	Density (gm/cm^3)	Error in Recorded Height (%)
1	1.02176	0.3
5	1.02201	0.3
10	1.02231	0.3
20	1.02293	0.2
30	1.02354	0.1
40	1.02416	0.1
50	1.02477	0.1
100	1.02784	0.3
200	1.03415	0.9
300	1.04038	1.5
400	1.04038	2.1
500	1.05283	2.7
1000	1.08314	5.3

Precision of this wave/fluid-mud pressure sensing system is excellent. According to the manufacturer, total error in pressure transducers, including linearity and hysteresis, is less than 0.35 percent over the 13-33 psi range. The electronic readout and strip-chart recorder each have a precision of 1 percent. If maximum error for the system is taken to be the sum of error for the components, then results are reproducible to within less than 2.5 percent.

Absolute accuracy of the system is unknown but is believed to be within 5 percent. Systematic errors in differential density measurements can result if $H_B - H_A$ is not accurately determined. Density changes resulting from the passage of waves are believed to be accurate to within 0.008 gm/cm^3, while long-term density changes are believed to be accurate to within 0.004 gm/cm^3.

APPENDIX II

Data Processing and Time Series Analysis

Digitizing

Wave and differential pressure data were collected as analogue signals on a strip-chart recorder. Each time series, of 20-min record length, was digitized using a Calmagraphic III digitizer (Calma Corporation), and this information was then stored on magnetic tape. The digital sampling increment of $\Delta t = 0.2$ sec gave 6000 data points per record and assured a sufficiently high Nyquist frequency, $f = 1/2\Delta t$, to preclude aliasing effects (Kinsman, 1965, p. 452). Error introduced by high-frequency unsteady hand movements was assumed negligible.

Wave Spectral Analysis

Spectral analysis is an analytical tool for obtaining essential information from time series records. The pioneering work by Tukey (1949, 1958, 1961) formed a base from which later applications were taken (Bendat and Piersol, 1966; Kisel, 1969; Edge and Liu, 1970).

Given a stationary process with $\eta(t)$ as the randomly fluctuating signal, then the convolution of $\eta(t)$ with itself at a given lag τ forms the autocorrelation function, defined as

$$r_T(\tau) = \frac{1}{2T} \int_{-T}^{T} \eta(t)\eta(t+\tau)\, dt \,. \tag{II.1}$$

The Fourier transform of the autocorrelation function is the sample spectral density function

$$R_T(\sigma) = 2 \int_{0}^{\infty} r_T(\tau) \exp(i2\pi\sigma\tau)\, d\tau \,. \tag{II.2}$$

Variance, defined as the average squared deviation of observations from their mean, is for a process of zero mean, equal to the average $\eta(t)^2$. Further,

$$\text{Var} = \int_{0}^{\infty} R_T(\sigma)\, d\sigma. \tag{II.3}$$

Thus total variance of an energy spectrum is equal to the total area under all spectral peaks; in small-amplitude wave theory, this energy is proportional to the square of wave amplitude. From this knowledge it is possible to gain important information about the distribution of wave energy as a function of frequency.

Wave spectral analyses were performed using a Biomedical Time Series Program (BMDO2T), modified to handle 10^4 data points. As suggested by Kinsman (1965, p. 446), the number of lags selected, m, was always less than 0.1N, one-tenth the number of sample points. Prior to analysis, each record was detrended to remove the effect of an increase or decrease in

water depth owing to changing tide.

Care must be taken when interpreting a wave spectrum. Although an underlying assumption is stationarity, in reality a 20-min time series may be too short to adequately characterize a process of time length infinity. Further, difficulties may arise when trying to resolve sinusoidal components from signals that are strongly nonsinusoidal. With periodic sea surface elevations that are above but not below a SWL "trough" elevation, as in pure solitary waves, harmonic spectral peaks arise. Although the variance of a wave spectrum is a conservative property, the derived height information is not, and harmonic energy peaks do not represent true sea surface elevations.

APPENDIX III

Sample Analysis

Water Samples

Water samples were collected in a 1-liter modified Van Dorn bottle, stored in airtight 500-ml plastic containers, then returned to the laboratory for analysis. Suspended-sediment concentration and salinity were determined for each sample.

Samples of 30-300 ml were filtered through preweighed 0.45micron, 47-mm diameter Millipore membrane filters using a pressure filtration system. Preliminary laboratory investigations indicated that a stacked filter system to account for leaching was not necessary owing to the small volumes of water filtered (Eaton et al., 1969). After filtering, each filter pad was washed three times with 10 ml of distilled water to remove salts, air dried at 25°C for 48 hours, desiccated for 1 hour, and weighed to the nearest 0.01 mg. Suspended sediment concentration was then calculated and expressed as mass of dried sediment per volume of solution. The precision of this method depends on concentration of the sample; however, the coefficient of variation (standard deviation/mean) was less than 3 percent.

Salinity was determined from the filtrate of each sample using a Mark IV conductive salinometer (Lab Line Instruments, Inc.). With this instrument, accuracy is a function of conductivity. According to the manufacturer, accuracy is better than ± 0.5 °/∞ at 35 °/∞ and ± 0.1 °∞/ at 10 °/∞ .

Fluid-Mud Samples

"Suspensions" with concentrations greater than 10,000 mg/l are generally referred to as fluid mud (Krone, 1962) and cannot be analyzed by standard filtration techniques. To determine concentration of fluid-mud samples, 50 ml of solution were carefully measured from a volumetric flask, rinsed four times with distilled water to remove salts, the excess being decanted each time, then oven dried at 80° C. After cooling, the sample was weighed at room humidity to the nearest 0.01 mg and the concentration expressed as mass of solids per volume of solution.

Bulk density, defined as total mass of sample per volume of solution, can be determined in the laboratory by weighing a known volume of fluid mud. However, precision is poor since small volume errors can introduce large weight errors. Overall precision is improved by taking the specific volume of sediment (0.377 cm^3/gm for particle density of 2.65 gm/cm^3) and determining the amount of seawater that will be displaced for a given concentration, as determined above. For example, sediment particles in fluid mud with a concentration of 100,000 mg/l in seawater of density 1.025 gm/cm^3 will displace 38.6783 gm of water, assuming particle density is 2.65 gm/cm^3. Bulk density is then calculated (per liter of solution) as

(initial mass of seawater) - (mass of water displaced)

$$1025 \text{ gm} - 38.68 \text{ gm} + (\text{mass of sediment}) \qquad \text{(III.1)}$$

$$100 \text{ gm} = 1086 \text{ gm}$$

This corresponds to a bulk density of 1.086 gm/cm^3. Following a similar procedure, water content, given as

[(mass of sample - mass of solids)/(mass of solids + salts)] x 100

$$[\ (1086 \text{ gm} - 100 \text{ gm}) \div (100 \text{ gm} + 25 \text{ gm})\ ] \times 100 \qquad \text{(III.2)}$$

$$= 709\%$$

can be determined without weighing a measured volume. Mass of salts must be known from a salinity determination. Since the void spaces in a marine sediment are assumed to be water-saturated, voids ratio is given by

$$e = \frac{\text{Volume of voids}}{\text{Volume of solids}} = \frac{\text{Specific gravity x water content}}{100} \qquad \text{(III.3)}$$

Richards et al. (1974) have found, from analysis of more than 1500 marine sediment samples, that the linear relationship between voids ratio and water content gives an average specific gravity of 2.72.

Viscosity was determined graphically from curves prepared by NEDECO (1965) that were based on more than 4000 viscosity measurements made on fluid mud and soil samples from Surinam and British Guiana using a Brookfield viscometer. Viscosity is a function of sediment concentration, salinity, and shearing rate. Values reported in the present study are for seawater of salinity 35 °/$_{\infty}$ and shearing rate of 10 rpm for a duration of 6 min.

Particle size distributions were determined from pipette analyses following standard procedures given by Folk (1968). Approximately 15 gm of sediment (wet weight) were disaggregated in a blender filled halfway with 10 percent calgon dispersant solution, then poured into a graduated cylinder and brought to exactly the 1000-ml mark with dispersant solution. Each cylinder was left for 24 hours to check for flocculation. Withdrawals were made at appropriate times and depths (assuming Stokes settling velocity) and released into evaporating dishes for drying. Pipette withdrawals were terminated at 11ϕ (0.5 micron), since a constant temperature could not be assured past this point. Each sample was desiccated and weighed, a calgon correction was subtracted, and the weight percentage was determined.

REFERENCES

Allersma, E., 1968, Mud on the oceanic shelf off Guyana. Paper contributed to Symposium on Investigations and Resources of the Caribbean Sea and Adjacent Regions, CICAR Conference, Curacao (Delft Hydraulics Laboratory, Delft, The Netherlands, unpublished), 20 pp.

Allersma, E., A. J. Hoekstra, and E. W. Bijker, 1967, Transport patterns in the Chao Phya estuary. Delft Hydraulics Laboratory, Delft, The Netherlands, Publication No. 47.

Ariathurai, R., and R. B. Krone, 1975, Mathematical modeling of sediment transport in estuaries. In (M. Wiley, ed.) Estuarine processes, vol. II, Circulation, sediments, and transfer of material in the estuary. New York (Academic Press), pp. 98-106.

Bagnold, R. A., 1963, Mechanics of marine sedimentation. In (M. N. Hill, ed.) The sea. New York (Wiley Interscience), 3:507-528.

Bates, C. C., 1953, Rational theory of delta formation. Bull. Am. Assoc. Petrol. Geologists, 37:2119-2162.

Bea, R. G., H. A. Bernard, P. Arnold, and E. H. Doyle, 1975, Soil movements and forces developed by wave-induced slides in the Mississippi Delta. J. Petrol. Tech., pp. 500-514.

Bendat, J. S., and A. G. Piersol, 1966, Measurement and analysis of random data. New York (John Wiley and Sons), 390 pp.

Boussinesq, J., 1872, Théorie des ondes et de remous qui se propagent le long d'un canal rectangulaire horizontal, en communiquant au liquide contenu dans ce canal des vitesses sensiblement paralleles de la surface au fond. J. Math. Pures et Appliquées, 17:55-108.

Bristow, R. C., 1938, Cochin harbour development: history of mud banks, vol. I. Ernakulam, India (Cochin Government Press), 174 pp.

Coastal Engineering Research Center, 1973, Shore protection manual. U.S. Army Corps of Engineers, Washington, D.C., 3 vol.

Daily, J. W., and S. C. Stephan, Jr., 1953a, The solitary wave--its celerity, profile, internal velocities and amplitude attenuation in a horizontal smooth channel. Proc., 3rd Conf. Coastal Engr., Cambridge, Mass., pp. 13-30.

Daily, J. W., and S. C. Stephan, 1953b, Characteristics of the solitary wave. Trans. Am. Soc. Civil Engrs., 118:575-587.

Delft Hydraulics Laboratory, 1962, Demerara coastal investigation. Delft, The Netherlands, 240 pp.

Dolan, R., B. Hayden, G. Hornberger, J. Zieman, and M. Vincent, 1972, Classification of the coastal environments of the world, part I, the Americas. Dept. Environmental Sciences, Univ. Virginia, Tech. Rept. I, 163 pp.

Doyle, E. H., 1973, Soil-wave tank studies of marine soil instability. Preprint 1901, Fifth Offshore Tech. Conf., Houston, pp. II-753 - II-766.

Drake, D. E., 1976, Suspended sediment transport and mud deposition on continental shelves. In (D. J. Stanley and D. J. P. Swift, ed.) Marine sediment transport and environmental management. New York (Wiley Interscience), pp. 127-158.

Eaton, J. S., G. E. Likens, and F. H. Bormann, 1969, Use of membrane filters in gravimetric analyses of particulate matter in natural waters. Water Resources Res., 5:1151-1156.

Edge, B. L., and P. C. Liu, 1970, Comparing power spectra computed by Blackman-Tukey and Fast Fourier Transform. Water Resources Res., 6:1601-1610.

Eisma, D., 1967. Oceanographic observations on the Surinam shelf. Hydrographic Newsletter, Spec. Pub. 5, pp. 21-53.

Eisma, D., and H. W. van der Marel, 1971, Marine muds along the Guyana coast and their origin from the Amazon Basin. Contributions Mineralogy and Petrology, 31:321-334.

Fisk, H. N., E. McFarlan, and C. R. Kolb, 1954, Sedimentary framework of the modern Mississippi delta. J. Sediment. Petrol., 24:76-99.

Folk, R. L., 1968, Petrology of sedimentary rocks. Austin, Texas (Hemphill's), 17[illegible]

Gade,H. G., 1958, Effects of a nonrigid, impermeable bottom on plane surface waves in shallow water. J. Marine Res., 16:61-82.

Gade,H. G., 1959, Notes on the effect of elasticity of bottom sediments to the energy dissipation of surface waves in shallow water. Arch. Math. Natur., Oslo, 55:69-80.

Gibbs, R. J., 1967, Geochemistry of the Amazon River system. Part I. The factors that control the salinity and the composition and concentration of the suspended solids. Bull. Geol. Soc. Am., 78:1203-1232.

Gibbs, R. J., 1975, Distribution and transport of suspended particulate material of the Amazon River in the ocean. In (M. Wiley, ed.) Estuarine processes, v. II, Circulation, sediments and transfer of material in the estuary. New York (Academic Press), pp. 35-47.

Gibbs, R. J., 1976, Amazon River sediment transport in the Atlantic Ocean. Geology, 4:45-48.

Goldsmith, V., 1976, Wave climate models for the continental shelf: critical links between shelf hydraulics and shoreline processes. In (R. A. Davis, Jr., and R. L. Ethington, eds.) Beach and nearshore sedimentation. Soc. Econ. Paleont. and Mineral., Tulsa, pp. 24-47.

Hjulstrom, F., 1935, Studies of morphological activity of rivers as illustrated by the River Fyris. Bull. Geol. Inst. Upsala, v. 25.

Hough,S. S., 1896, On the influence of viscosity on waves and currents. Proc. London Math. Soc., 28:264-288.

Hunt, J. N., and A. H. Brampton, 1972, Effect of friction on wave shoaling. J. Geophys. Res., 77:6558-6564.

Hydraulic Research Division, Ministry of Public Works and Traffic, 1970, Quality and availability of river water in coastal areas of Surinam. Paramaribo, Surinam, 175 pp.

Inglis, C. C., and F. H. Allen, 1957, The regimen of the Thames as affected by currents, salinities and river flow. Proc. Inst. Civ. Engrs., 7:827-878.

Ippen, A. T., 1966, Sedimentation in estuaries. In (A. T. Ippen, ed.) Estuary and coastline hydrodynamics. New York (McGraw-Hill), Chapt. 15, pp. 648-672.

Ippen, A. T., and Kulin, G., 1955, The shoaling and breaking of the solitary wave. Proc., 5th Conf. Coastal Engr., Grenoble, pp. 27-49.

Ippen, A. T., G. Kulin, and M. A. Raza, 1955, Damping characteristics of the solitary wave. Hydrodynamics Laboratory, Mass. Inst. Tech., Tech. Rept. 16, 40 pp.

Johnson, J. W., 1956, Dynamics of nearshore sediment movement. Bull. Am. Soc. Petrol. Geologists, 40:2211-2232.

Johnson, J. W., 1957, The littoral drift problem at shoreline harbors. J. Waterways and Harbors Div., Am. Soc. Civ. Engrs., 83:1-37.

Keulegan, G. H., 1948, Gradual damping of solitary waves. J. Res. NBS, 40:487.

Keulegan, G. H., 1950, Wave motion. In (H. Rouse, ed.) Engineering hydraulics. New York (Wiley Interscience), Chapt. 11, pp. 711-768.

Kinsman, B., 1965, Wind waves. Englewood Cliffs, New Jersey (Prentice-Hall), 676 pp.

Kirby, R., and W. R. Parker, 1973, Fluid mud in the Severn estuary and Bristol channel and its relevance to pollution studies. Preprint, Annual Symposium, Inst. Chem. Engr., 14 pp.

Kisel,C. C., 1969, Time series analysis of hydrologic data. Advances in Hydroscience, 5:1-112.

Komar, P. D., 1976, Beach processes and sedimentation. Englewood Cliffs, New Jersey (Prentice-Hall), 429 pp.

Krone, R. B., 1962, Flume studies of the transport of sediment in estuarial shoaling processes. Univ. California Hydraulic Engr. Lab. and Sanitary Research Lab., Berkeley, 110 pp.

Krone, R. B., 1972, A field study of flocculation as a factor in estuarial shoaling processes. Committee on Tidal Hydraulics, Corps of Engrs., Vicksburg, Miss., Tech. Rept. 16, 62 pp.

Lamb, H., 1932, Hydrodynamics, 6th ed. Cambridge (Cambridge Univ. Press), 738 pp.

Lhermitte, P., 1958, Bulletin d'information, comite d'oceanographique et d'etudes des cotes, v. 10, no. 5.

Lhermitte, P., 1960, Mouvements des materiaux de fond sous l'action de la houle. Proc., 7th Conf. Coastal Engr., The Hague, pp. 211-261.

Madsen, O. S., 1976, Wave climate of the continental margin:- elements of its mathematical description. In (D. J. Stanley and D. J. P. Swift, eds.) Marine sediment transport and environmental management. New York (Wiley Interscience), pp. 65-87.

McCave, I. N., 1971, Wave effectiveness at the sea bed and its relationship to bed-forms and deposition of mud. J. Sediment. Petrol., 41:89-96.

McCave, I. N., 1972, Transport and escape of fine-grained sediment from shelf areas. In (D. J. P. Swift, D. B. Duane, and O. H. Pilkey, eds.) Shelf sediment transport: process and pattern. Stroudsburg, Pa. (Dowden, Hutchinson and Ross), pp. 225-248.

McClelland, B., 1967, Progress of consolidation in delta front and prodelta clays of the Mississippi River. Marine Geotechnique, Urbana (Univ. of Illinois Press), pp. 22-40.

McCowan, J., 1894. On the highest wave of permanent type. Phil. Mag., series 5, 38:351-357.

Meade, R. H., P. L. Sachs, F. T. Manheim, J. C. Hathaway, and D. W. Spencer, 1975, Sources of suspended matter in waters of the Middle Atlantic Bight. J. Sediment. Petrol., 45:171-188.

Metcalf, W. G., 1968, Shallow currents along the northeastern coast of South America. J. Marine Res., 26:232-243.

Migniot, C., 1968, A study of the physical properties of various forms of very fine sediment and their behavior under hydrodynamic action. La Houille Blanche, No. 7, pp. 591-620.

Moni, N. S., 1970, Study of mudbanks along the southwest coast of India. Proc., 12th Conf. Coastal Engr., Washington, D.C., 2:739-750.

Morgan, J. P., J. R. van Lopik, and L. G. Nichols, 1953, Occurrence and development of mudflats along the western Louisiana coast. Coastal Studies Inst., Louisiana State Univ., Tech. Rept. 2, 34 pp.

Munk, W. H., 1949, The solitary wave theory and its applications to surf problems. Ann. N. Y. Acad. Sci., 51:376-424.

Nair, R. R., 1976, Unique mud banks, Kerala, Southwest India. Bull. Am. Assoc. Petrol. Geologists, 60:616-621.

NEDECO, 1965, A study on the siltation of the Bangkok port channel, v. II. Netherlands Engr. Consultants, The Hague, 474 pp.

NEDECO, 1968, Surinam transportation study. Netherlands Engr. Consultants, The Hague, 293 pp.

Odd, N. V. M., and M. W. Owen, 1972, A two-layer model of mud transport in the Thames estuary. Proc. Inst. Civ. Engrs., Supplement Paper #7517S, pp. 175-205.

Owen, M. W., 1969, A detailed study of the settling velocities of an estuary mud. Hydraulics Research Station, Wallingford, England, Rept. No. INT 78, 40 pp.

Owen, M. W., 1970, Properties of a consolidating mud. Hydraulics Research Station, Wallingford, England, Rept. No. INT 83, 90 pp.

Partheniades, E., 1971, Erosion and deposition of cohesive materials. In (H. W. Shen, ed.) River mechanics. Boulder (Colorado State Univ. Press), pp. 25-1-25-91.

Pierce, T. J., and D. J. Williams, 1966, Experiments on certain aspects of sedimentation of estuarine muds. Proc. Inst. Civ. Engrs., 34:391-402.

Putnam, J. A., and J. W. Johnson, 1949, The dissipation of wave energy by bottom friction. Trans. Am. Geophys. Union, 30:67-74.

Richards, A. F., J. T. Hirst, and J. M. Parks, 1974, Bulk density-water content relationship in marine silts and clays. J. Sediment. Petrol., 44:1004-1009.

Simmons, H. B., 1966, Field experience in estuaries. In (A. T. Ippen, ed.) Estuary and coastline hydrodyamics. New York (McGraw-Hill). Chapt. 16, pp. 673-690.

Sonu, C. J., 1972, Field observation of nearshore circulation and meandering currents. J. Geophys. Res., 77:3232-3247.

Suhayda, J. N., T. Whelan, III, J. M. Coleman, J. S. Booth, and L. E. Garrison, 1976, Marine sediment instability: interaction of hydrodynamic forces and bottom sediments. Preprint 2426, Eighth Offshore Tech. Conf., Houston, pp. 29-40.

Sundborg, A., 1956, The River Klaralven: a study of fluvial processes. Geogr. Ann., 38:125-316.

Tubman, M. W., and J. N. Suhayda, 1976, Wave action and bottom movements in fine sediments. Proc., 15th Conf. Coastal Engr., Honolulu, 2:1168-1183.

Tukey, J. W., 1949, The sampling theory of power spectrum estimates. In Symposium on Applications of Autocorrelation Analysis to Physical Problems, Woods Hole, NAVEXOS-P-735, Office of Naval Research, Washington, D.C., pp. 45-67.

Tukey, J. W., 1958, The estimation of (power) spectra and related quantities. In (R. E. Langer, ed.) On Numerical Approximation, Proceedings, Symposium conducted by the Mathematics Research Center, U.S. Army, at the Univ. of Wisconsin, Madison. Univ. of Wisconsin Press, pp. 389-411.

Tukey, J. W., 1961, Discussion, emphasizing the connection between analysis of variance and spectrum analysis. Technometrics, 3:191-228.

Vann, J. H., 1959, The physical geography of the lower coastal plain of the Guiana coast. Dept. Geography and Anthropology, Louisiana State Univ., Tech. Rept. 1, 91 pp.

Wells, J. T., and J. M. Coleman, 1977, Nearshore suspended sediment variations, central Surinam coast. Marine Geology, 24:M47-M54.

Whitehouse, U. G., and L. K. Jeffrey, 1954, Flocculation in estuaries. API Research Project 51, Texas A & M Research Foundation, College Station, Texas.

Zenkovitch, V. P., 1967, Processes of coastal development. New York (Wiley Interscience), 738 pp.

Zonneveld, J. I. S., 1954, Observations along the coast of Surinam. Tijdschr. Kon. Ned. Aardr. Gen., 71:18-31.

Unclassified Distribution List
Reports of Contract N00014-75-C-0192,
Project NR 388 002

Office of Naval Research
Geography Programs
Code 462
Arlington, Virginia 22217

Defense Documentation Center
Cameron Station
Alexandria, Virginia 22314

Director, Naval Research Lab
Attn: Technical Information Officer
Washington, D.C. 20375

Director
Office of Naval Research Branch Office
1030 East Green Street
Pasadena, California 91101

Director
Office of Naval Research Branch Office
536 South Clark Street
Chicago, Illinois 60605

Director
Office of Naval Research Branch Office
495 Summer Street
Boston, Massachusetts 02210

Commanding Officer
Office of Naval Research Branch Office
Box 39
FPO New York 09510

Chief of Naval Research
Asst. for Marine Corps Matters
Code 100M
Office of Naval Research
Arlington, Virginia 22217

Office of Naval Research
Operational Applications Div.
Code 200 Arlington, Virginia 22217

Office of Naval Research
Scientific Liaison Officer
Scripps Inst. of Oceanography
La Jolla, California 92038

Director, Naval Research Lab
Attn. Library, Code 2628
Washington, D.C. 20375

Commander
Naval Oceanographic Office
Attn. Library, Code 1600
Washington, D.C. 20374

Naval Oceanographic Office
Code 3001
Washington, D.C. 20374

Chief of Naval Operations
OP 987P1
Department of the Navy
Washington, D.C. 20350

Oceanographer of the Navy
Hoffman II Building
200 Stovall Street
Alexandria, Virginia 22322

Naval Academy Library
U.S. Naval Academy
Annapolis, Maryland 21402

Commanding Officer
Naval Coastal Systems Laboratory
Panama City, Florida 32401

Librarian
Naval Intelligence Support Center
4301 Suitland Road
Washington, D.C. 20390

Office of Naval Research
Code 480
National Space Technology Lab
Bay St. Louis, MS 39520

Commanding Officer
Naval Civil Engineering Lab
Port Hueneme, California 93041

Officer in Charge
Environmental Prediction Research Facility
Naval Post Graduate School
Monterey, California 93940

Dr. Warren C. Thompson
Dept. of Meteorology and Oceanography
U.S. Naval Post Graduate School
Monterey, California 93940

Director
Amphibious Warfare Board
U.S. Atlantic Fleet
Naval Amphibious Base
Norfolk, Little Creek, Va. 23520

Commander, Amphibious Force
U.S. Pacific Fleet
Force Meteorologist
COMPHIBPAC CODE 25 5
San Diego, California 92155

Commanding General
Marine Corps Development and Educational Command
Quantico, Virginia 22134

Dr. A. L. Slafkosky
Scientific Advisor
Commandant of the Marine Corps
Code MC-RD-1
Washington, D.C. 20380

Defense Intelligence Agency
Central Reference Division
Code RDS-3
Washington, D.C. 20301

Director
Coastal Engineering Res. Center
U.S. Army Corps of Engineers
Kingman Building
Fort Belvoir, Virginia 22060

Chief, Wave Dynamics Division
USAE-WES
P.O. Box 631
Vicksburg, Miss. 39180

Commandant
U.S. Coast Guard
Attn: GECV/61
Washington, D.C. 20591

Office of Research and Development
c/o DS/62
U.S. Coast Guard
Washington, D.C. 20591

National Oceanographic Data Center c/o D764
Environmental Data Services
NOAA
Washington, D.C. 20235

Central Intelligence Agency
Attn: OCR/DD-Publications
Washington, D.C. 20205

Dr. Donald Swift
Marine Geology and Geophysics Laboratory
AOML - NOAA
15 Rickenbacker Causeway
Miami, Florida 33149

Dr. Hsiang Wang
Dept. of Civil Engineering
Dupont Hall
University of Delaware
Newark, Delaware 19711

Ministerialdirektor
Dr. F. Wever
Rue/FO
Bundesministerium der
Verteidigung
Hardthoehe
D-5300 Bonn, West Germany

Oberregierungsrat
Dr. Ullrich
Rue/FO
Bundesministerium der
Verteidigung
Hardthoehe
D-5300 Bonn, West Germany

Dr. Yoshimi Goda
Director, Wave Research Div.
Port and Harbor Research Inst.
Ministry of Transportation
1-1 Nagase, 3 Chome
Yokosuka, 239 Japan

Mr. Tage Strarup
Defence Research Establishment
Osterbrogades Kaserne
DK-2100 Kobenhavn O, Denmark

Prof. Dr. Rer. Nat. H. G.
Gierloff-Emden
Institut F. Geographie
Universitaet Muenchen
Luisenstrasse 37/III
D-800 Muenchen 2, West Germany

Prof. Dr. Eugen Seibold
Geol-Palaeontolog. Institut
Universitaet Kiel
Olshausenstrasse 4-60
D-2300 Kiel, West Germany

Dr. R. Koester
Geo.-Palaeontolog. Institut
Universitaet Kiel
Olshausenstrasse 40-60
D-2300 Kiel, West Germany

Prof. Dr. Fuehrboeter
Lehrstuhl F. Hydromechanik U.
Kuestenwasserbau
Technische Hochschule
Braunschweig
Beethovenstrasse 51A
D-3300 Braunschweig
West Germany

Prof. Dr. Walter Hansen
Direktor D. Instituts f.
Meereskunde
Universitaet Hamburg
Heimhuderstrasse 71
D-2000 Hamburg 13,
West Germany

Prof. Dr. Klaus Hasselmann
Institut F. Geophysik
Universitaet Hamburg
Schuleterstrasse 22
0-2000 Hamburg 13, West Germany

Prof. Dr. Nils Jerlov
Institute for Physical
Oceanography
Kobenhavns Universitet
Haraldsgade 6
DK-2200 Kobenhavn, Denmark

Mr. William T. Whelan
Telecommunication Ent. Inc.
Box 88
Burtonsville, MD 20730

Dr. H. J. Schoemaker
Waterloopkundig Laboratorium
Te Delft
61 Raam, Delft, Netherlands

Ir. M. W. Van Batenberg
Physisch Laboratorium TNO
Oude Waalsdorper Weg 63, Den Haag
Netherlands

Dr. J. Ernest Breeding, Jr.
Dept. of Oceanography
Florida State University
Tallahassee, Florida 32306

Dr. John C. Kraft
Dept. of Geology
University of Delaware
Newark, Delaware 19711

Dr. Dag Nummedal
Dept. of Geology
University of South Carolina
Columbia, South Carolina
29208

ONR Scientific Liaison Group
American Embassy
Room A-407
APO San Francisco, CA 96503

Dr. Choule J. Sonu
Tetra Tech, Inc.
630 North Rosemead Blvd.
Pasadena, California 91107

Dr. Richard A. Davis, Jr.
Department of Geology
University of South Florida
Tampa, Florida 33620

Dr. William T. Fox
Department of Geology
Williams College
Williamstown, Mass. 01267

Dr. John Southard
Dept. of Earth and
Planetary Sciences
MIT
Cambridge, Massachusetts
02139

Dr. John T. Kuo
Henry Krumb School of Mines
Seeley W. Mudd Building
Columbia University
New York, New York 10027

Dr. Edward B. Thornton
Department of Oceanography
Naval Postgraduate School
Monterey, California 93940

Prof. C. A. M. King
Department of Geography
University of Nottingham
Nottingham, England

Dr. Douglas L. Inman
Scripps Institute of
Oceanography
La Jolla, California 92037

Prof. Toshiyuki Shigemura
Civil Engineering Dept.
National Defense Academy
1-10-20 Hashirimizu
Yokosuka 239, Japan

Prof. Yuji Iwagaki
Civil Engineering Dept.
Kyoto University
9 Shimogamo Zenbucho,
Sakyo-Ku
Kyoto, Japan

Prof. Kiyoshi Horikawa
Dept. of Civil Engineering
University of Tokyo
7-3-1, Hongo, Bunkyo-Ku
Tokyo 113, Japan

Dr. William W. Wood
Department of Geosciences
Purdue University
Lafayette, Indiana 47907

Dr. Alan W. Niedoroda
Director, Coastal Research
Center
University of Massachusetts
Amherst, Mass. 01002

Dr. Benno M. Brenninkmeyer,
S.J.
Dept. of Geology & Geophysics
Boston College
Chestnut Hill, Mass. 02167

Dr. Omar Shemdin
JPL-CALTECH
Mail Stop 183-501
4800 Oak Grove Drive
Pasadena, California 91103

Dr. Lester A. Gerhardt
Rennsselaer Polytechnic Inst.
Troy, New York 12181

Mr. Fred Thomson
Environmental Research Inst.
P.O. Box 618
Ann Arbor, Michigan 48107

Dr. Thomas K. Peucker
Simon Fraser University
Department of Geography
Burnaby 2, B.C., Canada

Dr. Robert Dolan
Department of Environmental
Sciences
University of Virginia
Charlottesville, VA 22903

Revised 12-12-77

Unclassified
Security Classification

DOCUMENT CONTROL DATA - R & D

(Security classification of title, body of abstract and indexing annotation must be entered when the overall report is classified)

1. ORIGINATING ACTIVITY *(Corporate author)*
Coastal Studies Institute
Louisiana State University
Baton Rouge, Louisiana 70803

2a. REPORT SECURITY CLASSIFICATION
Unclassified

2b. GROUP
Unclassified

3. REPORT TITLE
SHALLOW-WATER WAVES AND FLUID-MUD DYNAMICS, COAST OF SURINAM, SOUTH AMERICA.

4. DESCRIPTIVE NOTES *(Type of report and inclusive dates)*

5. AUTHOR(S) *(First name, middle initial, last name)*
John T. Wells

6. REPORT DATE
April 1978

7a. TOTAL NO. OF PAGES
56

7b. NO. OF REFS
83

8a. CONTRACT OR GRANT NO.
N00014-75-C-0192

b. PROJECT NO.
NR 388 002

c.

d.

9a. ORIGINATOR'S REPORT NUMBER(S)
Technical Report, No. 257

9b. OTHER REPORT NO(S) *(Any other numbers that may be assigned this report)*

10. DISTRIBUTION STATEMENT
Approved for public release; distribution unlimited.

11. SUPPLEMENTARY NOTES

12. SPONSORING MILITARY ACTIVITY
Geography Programs
Office of Naval Research
Arlington, Virginia 22217

13. ABSTRACT

Time series measurements of shallow-water waves and fluid-mud density variations, taken simultaneously with tide elevation and suspended sediment data, indicate that wave/fluid-mud interactions in the nearshore may be largely responsible for the present-day accumulation of fine-grained sediment on the open, unprotected coast of northeastern South America. Results of field experiments conducted along the central Surinam coast show that accumulations of fluid mud affect incoming swell by changing their form from sinusoidal to solitary-like and by preventing wave breaking except for occasional spilling. As long-period swell (T = 12-16 sec) propagates over shallow banks of fluid mud, the wave height to water depth ratio remains nearly constant at 0.23; the steady decrease in wave height with shoaling water depth indicates that substantial amounts of wave energy are lost to a fluid-mud bottom even though breaking does not occur. Evaluation of several mechanisms for the dissipation of wave energy reveals that attenuation of high-frequency waves (T < 3 sec) may be due to internal friction resulting from the extraordinarily high kinematic viscosity of muddy coastal waters, whereas longer period waves may lose energy to viscous shear within a bottom boundary layer. (U)

A specially designed wave/fluid-mud pressure-sensing system indicates that fluid-mud density fluctuates by 0.025 to 0.05 gm/cm^3 on a wave-by-wave basis. As each wave crest passes the sensing instrument, a cloud of sediment with particle concentration of approximately 50,000 mg/l is suspended instantly; rapid settling that follows is explained by the formation of a collapsing interface. Wave-by-wave sediment suspension is superimposed on a longer term suspension and deposition process that is related to stage of the tide. Surface suspensate concentrations may exceed 3500 mg/l during this exchange process. (U)

Utilizing the concept of wave-associated currents, it has been shown, in taking angle of wave approach, average observed concentration of sediment in suspension, and net drift as given by solitary wave theory, that volume transports of 3 to 70 x 10^6 m^3/yr can be explained by waves alone. If a hypothesis of mud transport by solitary waves is accepted, then the continuous shoreward transport of suspended fluid mud, combined with the high rate of wave energy dissipation, explains in part the ability of muddy coasts to protect their shorelines. (U)

DD FORM 1 NOV 65 1473 (PAGE 1)
S/N 0101-807-6811

Unclassified
Security Classification

A-31408

086 700

14. KEY WORDS	LINK A		LINK B		LINK C	
	ROLE	WT	ROLE	WT	ROLE	WT
Shallow-water waves						
Fluid-mud dynamics						
Surinam, South America						
Wave/fluid-mud interactions						
Solitary waves						